Manon R. O. Ligeon

# Effective bactericidal nanopillars for *E. coli* and *S. aureus*

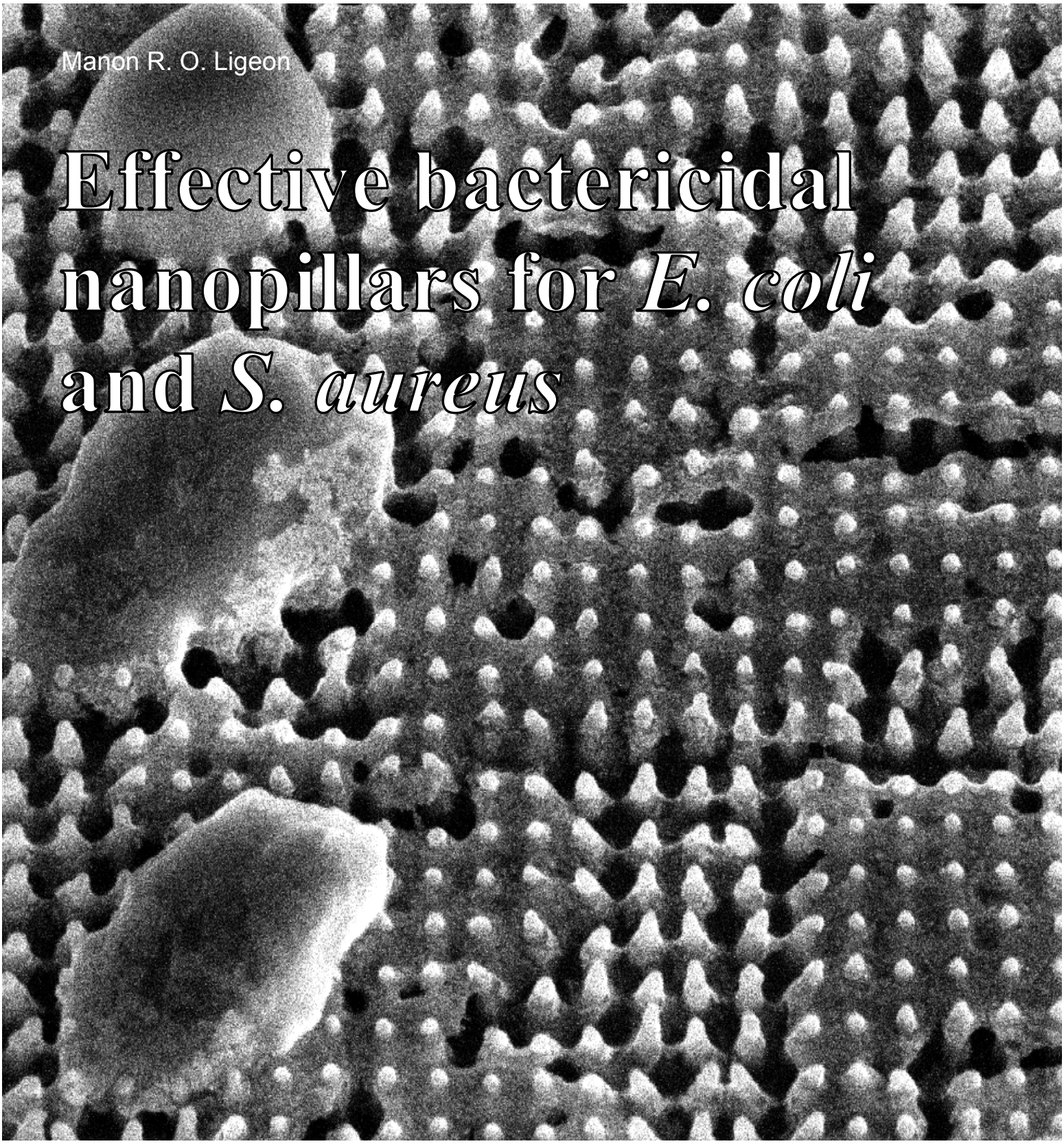

TU Delft

# Effective bactericidal nanopillars for *E. coli* and *S. aureus*

By

Manon Rachel Odilia Ligeon

in partial fulfilment of the requirements for the degree of

**Master of Science**
in Biomedical Engineering

at the Delft University of Technology,
to be defended publicly on Monday July 16, 2018 at 09:00 AM

Supervisors:

| | |
|---|---|
| Dr. ir. Lidy E. Fratila-Apachitei | TU Delft |
| Dr. Cornelis W. Hagen | TU Delft |
| Dr. Peter-Leon Hagedoorn | TU Delft |
| Dr. Linda G. Otten | TU Delft |
| Dr. ir. Iulian Apachitei | TU Delft |
| Prof. Dr. ir. Amir A. Zadpoor | TU Delft |

# Contents

## Abstract

Due to competition of host and bacterial cells to adhere and grow on implant surfaces, implants are frequently associated with a high risk of peri-implant infections. The microorganisms that are abundantly present during peri-implant infections are *Staphylococcus* bacteria and a variety of other less abundant bacteria as for example *Escherichia coli*. For this reason, some studies have been focusing on creating nanopatterns that might reduce bacterial colonization when used as implant surface topography. However, most of this research showed that the specified nanopatterns were only exceedingly bactericidal to either Gram-positive or Gram-negative bacteria. The aim of this novel study is to investigate the bactericidal effects of nanopatterns with pillar diameter of ~80 nm, a height of ~190 nm and an interpillar distance of ~170 nm on Gram-positive *Staphylococcus aureus* and Gram-negative *Escherichia coli*. The patterns were incubated with *S. aureus* and *E. coli* for 18 hours at 37 °C in their specific growth medium. The bactericidal effects were examined with scanning electron microscopy (SEM) by assessing the bacterial cell morphology and the amount of damaged bacterial cells found on the patterns. The patterns were able to damage approximately 96.9 ± 1.2% of *E. coli* and 83.9 ± 22.8% of *S. aureus* cells. The severity of bacterial cell damage has led to believe that the percentage of dead bacterial cells was a sufficient measure for the bactericidal efficacy of the pattern. Based on these results there is a convincing assumption that these specific pillar parameters can be used as a bactericidal surface topography on bone implants. Nevertheless, follow up experiments should be done in combination with live imaging of the cells to establish possible long-term bacterial- and host cell effects on topography and gain more insights into the proposed bactericidal mechanism(s).

## Acknowledgements

A lot of people were part of this master project, and without their help this thesis could not have been done. So, this is a shout out to all of you!
First, I'd like to thank all my supervisors: Lidy Fratila-Apachitei, Iulian Apachitei and Amir Zadpoor from Biomaterials and Tissue Biomechanics TU Delft, Cornelis (Kees) Hagen from Imaging Physics TU Delft and Linda Otten and Peter-Leon Hagedoorn from Biocatalysis TU Delft. I really appreciate that I was always able to drop by their office whenever I had questions and that they took the time to answer everything clearly. They also encouraged me to be more critical towards my own work by having room for discussion and improvement, which stimulated me to be a better researcher.

Special thanks to Aya Mahgoub, Khashayar Modaresifar and Mahya Ganjian, who guided me through every step of the project, were always available to help me out and had a lot of patience with me.
Furthermore, I'd like to thank Dustin Laur, Carel Heerkens, Laura Koekkoek-van der Weel and Jannie Kempff-Gruwel who were always available to support and assist me in the lab and provided me with sufficient training. Many thanks to Nazli Sarkalkan, who was of big help with the statistical analysis.

Last, but not least, I'd like to give my deepest appreciation to my parents, sister, brother-in-law and nephew. You were always there to motivate me through my studies, cheered me up when I was down and supported me no matter what.

# 1 Introduction

Due to competition of host and bacterial cells to adhere and grow on the surface of metallic bone implants, there exists a high risk of peri-implant infections. These are serious complications that are resistant to natural host defence mechanisms and most antibiotics, which means surgical intervention is one of the only treatments left. This can lead to disastrous consequences for patients, but also an increase in healthcare costs by more than 300% can be expected [1].

The microorganisms that are abundantly present during peri-implant infections are *Staphylococcus aureus* (34%), *Staphylococcus epidermidis* (32%), *Pseudonomas aeruginosa* (8%), *Enterococci* (5%), *Streptococcus viridans* (2%) and *Escherichia coli* (2%), but there are also a variety of other bacteria present (7%) for example: *Propionibacterium acnes, Lactobacillus, Haemophilus influenzae, Providencia, Citrobacter, Acinetobacter, Serratia marcescens* and *Corynebacterium* [1-3]. The other 10% of the bacterial infection is due to other staphylococcal species [3].

A lot of research has been done in creating antibacterial surfaces that might help prevent these peri-implant infections by adding this surface to the metallic bone implant [4]. The surface modification can be chemical or physical.

The addition of coatings, chemicals and free (silver) nanoparticles on the metallic bone implant are examples of chemical surface modification. However, this type of surface modification can lead to other serious complications for the patient [5, 6].
For example the release of nanoparticles in the body results in the development of reactive oxygen species that can activate oxidative stress and it can increase the occurrence of respiratory and cardiovascular disease [7].

However, most research regarding antibacterial properties is focused on the use of certain antibacterial coatings or antibacterial chemicals and nanoparticles and is not always related to Gram-positive bacteria like the *Staphylococcus* bacteria [8, 9].

For example, the nanopatterns OST2; OST2-H60 and OST2-SQ that were made in a recent study showed to be bactericidal towards *Escherichia coli*, which is less prominent at the implant infection site compared to the *Staphylococcus* bacteria [10].

The physical surface modification is mainly based on surface topography. When only changing the surface topography, the bacterial cells' mechanotransduction pathways can be activated to result in a certain tissue response independent of the surface chemistry.
This will have little to none additional adverse side effects regarding the patient, compared to the original bone implant without this specific (nano) topography added to the surface and it can provide a non-toxic alternative for the prevention of biofilm formation by either preventing the initial attachment of microorganisms (antibiofouling) or by physically exterminating them through the contact-killing implant-tissue interface (bactericidal) [6].

However, the mechanisms that lead to certain cell responses are not yet fully understood [7].
Recent topography-orientated experimental studies gave rise to the impression that nanostructures with a diameter in the range of 70-80 nm, height of 180-300 nm and interspace of 60-200 nm have bactericidal potential for both *S. aureus* and *E. coli* combined (*table 1).*

**Table 1: bactericidal pattern characteristics for *S. aureus* and *E. coli***

| Bacteria | Diameter [nm] | Height [nm] | Interspace [nm] |
|---|---|---|---|
| *S. aureus* | 70-100 | 100-1000 | 60-200 |
| *E. coli* | 70-80 | 180-300 | 60-380 |

For example, the combination of diameter 80 nm, large varying heterogeneous heights of ± 400 nm and interspace of 170 nm, was able to kill 100% of *S. aureus* cells. The nanopattern with the same properties but on average 200 nm lower pillar heights had a bactericidal efficacy of 98% against *S. aureus* [11].

The combination of diameter 70 nm, height 210 nm and interspace 100 nm, increased *E. coli* cell death by 117% compared to the flat surface [12] and the combination of diameter 60 nm, height 200 nm and interspace 170 nm, ruptured the cell wall of *P. aeruginosa* within 3 minutes after contact and led to cell death within 5 minutes after contact with the patterned surface [13].

A pattern with diameter of 80 nm, height of 350 nm and interspace of 250 nm, was bactericidal to *S. aureus* (50%), *P. aeruginosa* (25%) and *E. coli* (30%) [8].

Nanopillars with a diameter of 80.3 nm, height of 432.5 ± 63.5 nm and 99.5 nm interspace was able to kill 84% of *P. aeruginosa* and decrease their attachment by 70%. This same pattern killed 73% of *S. aureus* and decreased their attachment with 65%, which was determined by fluorescent staining in combination with inverted CSLM and SEM [14].

Another recent systematic study by Bhadra et al. showed that nanopillars (bSi-1) with a diameter of 100.1 ± 36 nm, height of 836.8 ± 91.2 nm and interspace of 153.1 ± 55.3 nm was able to kill 93% of *P. aeruginosa* and 92% of *S. aureus* was killed on a nanopillar pattern (bSi-2) with a diameter of 110.3 ± 26.9 nm, height of 657.9 ± 74.3 nm and interspace of 135.6 ± 33.9 nm. The bacterial adherence and viability was determined by using fluorescent dyes in combination with CSLM and SEM [15].

Based on these findings, we present a study of bactericidal properties of a specific topography, namely nanopillars with a base diameter of ~80 nm, tip diameter of ~20 nm, height of ~190 nm and interspace of ~170 nm. This pattern is produced with electron beam induced deposition (EBID). This production method results in a relatively precise controllability of the dimensions and high-resolution patterns [16].

The bactericidal effects are demonstrated with *S. aureus* and *E. coli* after 18 hours of incubation at 37 °C and examined with scanning electron microscopy (SEM) by assessing the bacterial cell morphology and the amount of damaged bacterial cells.

The results presented in this study indicate that this specific pattern can suffice as an effective bactericidal surface topography for both *E. coli* and *S. aureus*.

# 2 Materials and methods

## 2.1 Pattern generation by EBID

### 2.1.1 Sample preparations

Double sided polished silicon wafers (4 inches, thickness 525 ± 25 µm, (100), p-type, 0-100 Ohm cm) were used for this experiment. The silicon wafers were diced into 1x1 $cm^2$, called samples, in order to fit in the 24 well plates that were used in the bacterial experiments and is explained in the next paragraph.

After dicing the wafers, the samples were soaked for 15 minutes in nitric acid. This was followed by rinsing the samples two times with deionized water. Next, the samples were dried with compressed nitrogen gas and heated at 90℃ on the hot plate. By this way the contamination of the samples surfaces was kept to a minimum.

After the samples were completely dried they were spin coated with AZ5214 resist (liquid polymer) at 4000 RPM. This step was followed by baking the samples on a hotplate for 1 min at 110℃. Next, the resist on the edges of the samples was removed with acetone. Then an etching step was performed to etch the edges of the samples, consequently creating black silicon. The etching process was performed by *AMS100 Bosch* and took approximately 5 seconds. Afterwards, the samples were completely rinsed in acetone and spin-dried.

The small black silicon patterns on the edges were used to set up the resolution, focus, stigmatization, crossover and lens alignment prior to patterning. A sample without any pattern is hard to focus on with EBID. Having the correct focus is the most important aspect of using EBID for creating high-resolution patterns with precise features.

### 2.1.2 Pattern design and fabrication with EBID

One pattern type with specified dimension was created. This pattern type is nanopillars with a diameter of 80 nm, height of 190 nm and interpillar distance (from pillar centre to centre) of 170 nm (*figure 1, table 2*).
These dimensions fall in the bactericidal range for both *E. coli* and *S. aureus* (*table 1*) and studies with comparable dimensions have shown bactericidal effects against *E. coli* and *S. aureus* separately [11,13].
The pillars were deposited in a square arrangement (*figure 2*). This results in a pillar density of approximately 40 pillars per $\mu m^2$. Some studies suggested that the pillar density plays an important role in the bactericidal activity of the pattern [11, 14, 15].

The theory behind this is that the nanopillars cause substantial stress on the cell wall, which leads to an increase in the internal turgor pressure and cell wall stiffening. The cell membrane adheres onto the pillars and a region of the membrane is suspended between the pillars. If the cell membrane continues to adhere and sink down onto the surface, the surface area of the cell is increased and is extensively stretched between each nanopillar, which will eventually result in rupture [8, 9, 17, 18].

However, too little or too much pillars can discourage this process as was observed in the study of Wu et al, 2018. This study showed that the highest bactericidal activity for *S. aureus* was observed with patterns that exhibit an average pillar density of ~40 pillars per $\mu m^2$ [11].

**Table 2: specified bactericidal topography characteristics for *S. aureus* and *E. coli***

| Topography | Diameter [nm] | Height [nm] | Interpillar distance [nm] | Pillar density [n/ $\mu m^2$] |
|---|---|---|---|---|
| Nanopillars | 80 nm | 190 nm | 170 nm | 40 |

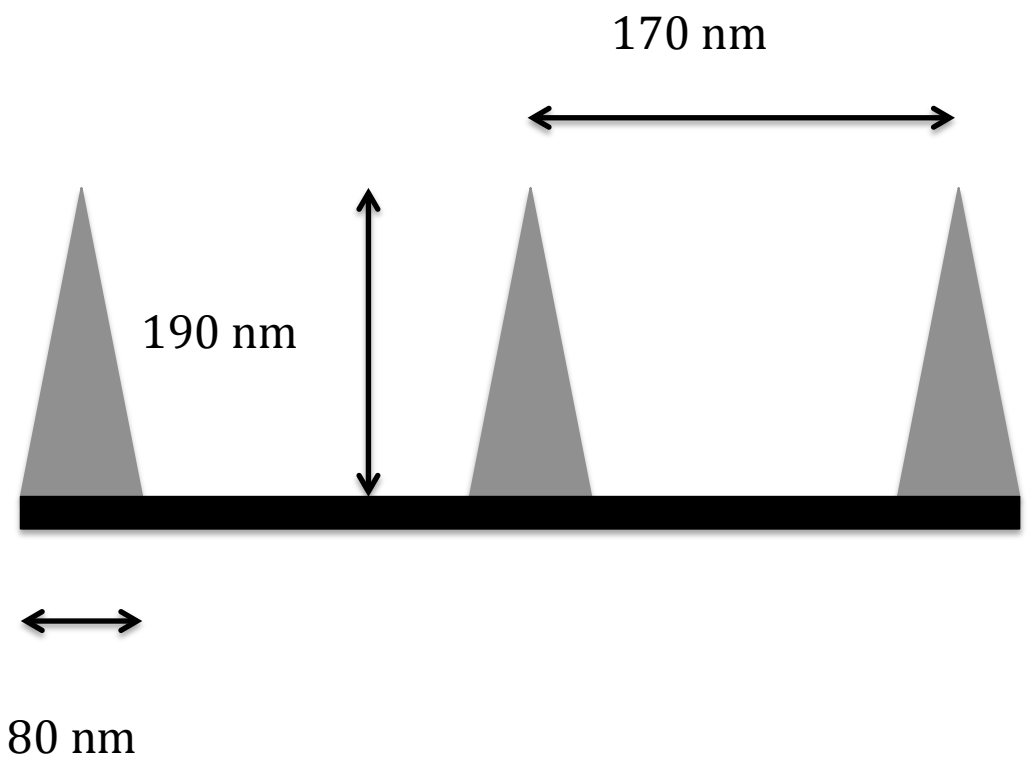


**Figure 1: Schematic representation of pillars including diameter, height and interpillar distance**

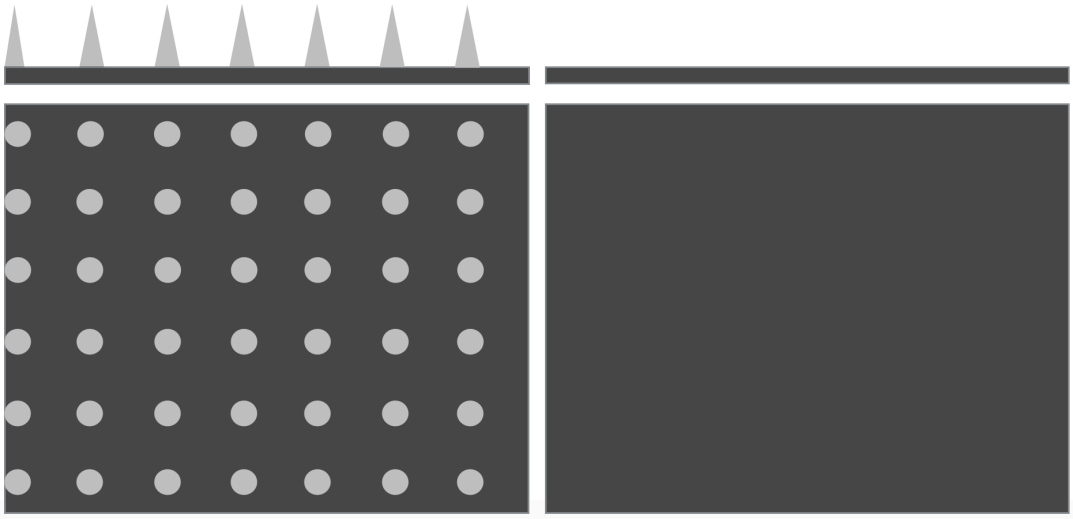

**Figure 2: Schematic representation of cross-section and top view of patterned surface and control surface**

Nine surfaces of each 42 x 42 $\mu m^2$ were patterned with these nanopillars on the samples.
Three of them were used for *E. coli* experiments and the other three were used for *S. aureus* experiments. The last three surfaces were used to show the reproducibility of the patterns with EBID.
The remaining non-patterned surfaces on the 1 x 1 $cm^2$ samples were used as control surfaces (Si control). In this way the difference between the bacterial interactions with the pattern versus with the non-patterned surfaces within one sample was investigated for the same bacterial culture. This was done for both *E. coli* experiments and *S. aureus* experiments.

There were also four other control surfaces that had no patterns on the sample. One of the control surfaces was incubated with *E. coli,* another one with *S. aureus,* the third one was placed in *E. coli* growth medium (no bacteria) and the fourth one in *S. aureus* growth medium (no bacteria).
The control surfaces without bacteria were used to secure the sterile working conditions. The control surfaces with bacteria were used to determine the correct optical density (OD) for the experiments. By testing different OD on smooth, non-patterned samples, an OD of 0.05 seemed to give the right amount of bacteria on the samples in order to evaluate bactericidal efficacy.

Lastly, there were two additional control surfaces that contained a thin layer of EBID deposition made of the same material as the nanopillars (Pt-C control). One of them was incubated with *E. coli* and the other one with *S. aureus*. The reason for these additional control samples was to assess the effect of the deposition material (platinum-carbon) on the bacterial cells.

In total there were fourteen surfaces investigated. The results of this study will focus on the six patterned surfaces, Si control and Pt-C control surfaces (*table 3*) in order to investigate the bactericidal efficacy of the patterns.

**Table 3: Overview of surfaces in combination with their characteristics and interactions**

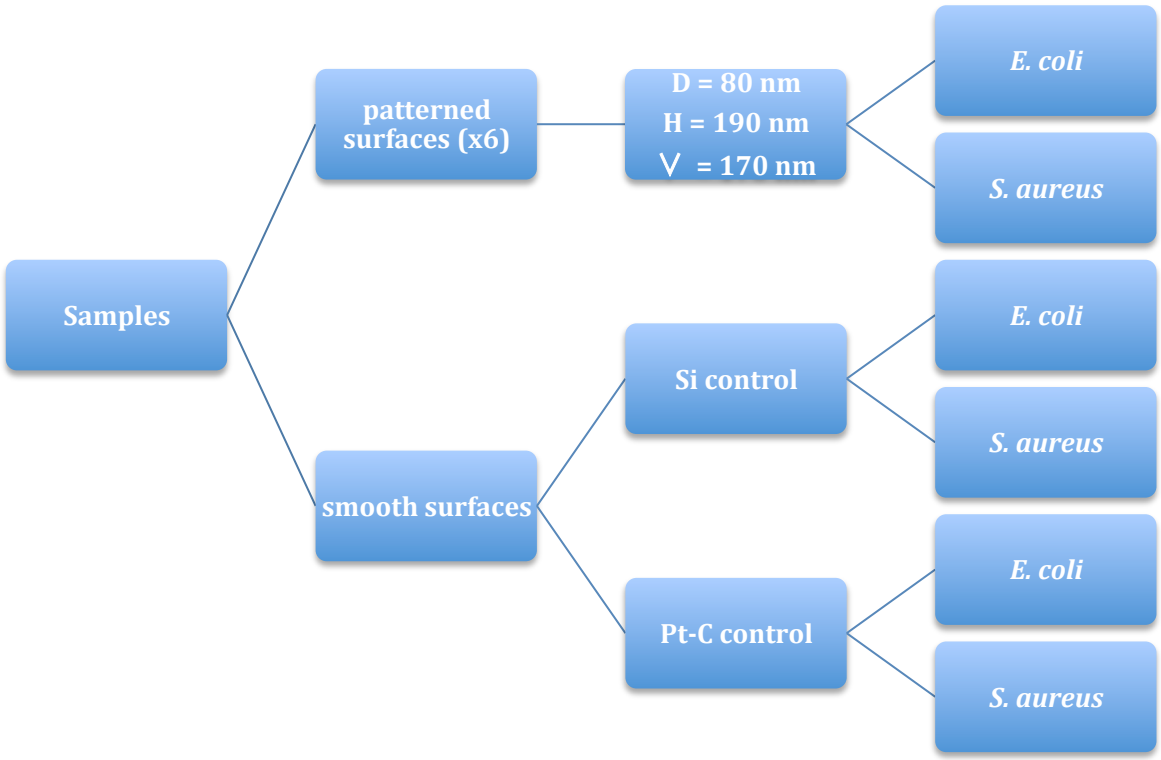

### 2.1.3 Pattern fabrication and EBID conditions

The patterns were created with the *Nova Nano Lab 650 Dual Beam system* of *FEI company* (*figure 3*). This machine, equipped with EBID and SEM, was used for deposition and imaging of the patterns.
With EBID it's possible to create controlled nanopatterns made of metallic material by directly depositing nanometer-scale structures on a substrate through electron-induced dissociation of adsorbed (metallic) precursor molecules [16, 19].

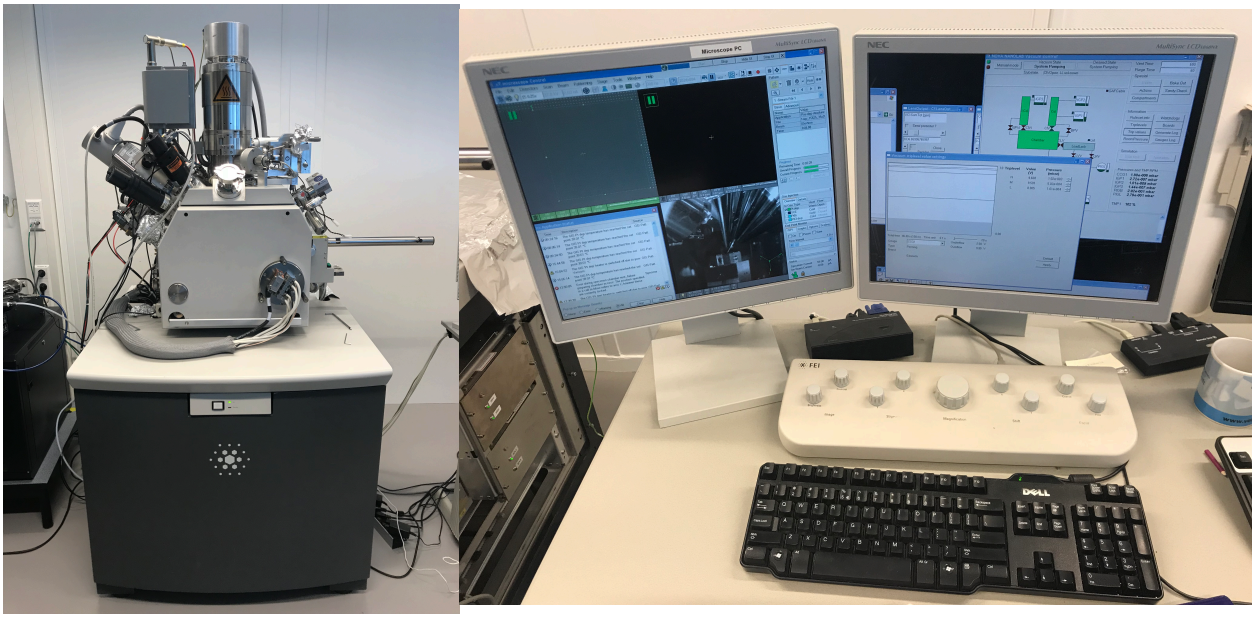

**Figure 3:** ***Nova Nano Lab 650 Dual Beam System*** **of** ***FEI company***

EBID was performed in immersion mode, ultrahigh resolution, with 17.8 kV electron beam voltage and 0.60 nA beam current. The contrast varied between 60.3 and 65.7 and the brightness between 46.5 and 46.8.
The background vacuum of the system was 8.82 $10^{-007}$ - 1.39 $10^{-006}$ mbar and the EBID process started at 1.80 $10^{-006}$ - 2.33 $10^{-006}$ mbar. The working distance was approximately 5 mm. The precursor gas was Trimethyl(methylcyclopentadienyl)-platinum(IV) $(CH_3C_5H_4)Pt(CH_3)_3$, MeCpPtIVMe$_3$ or $C_9H_{16}Pt$).
The gas nozzle/needle was inserted in every experiment and was located at 140 µm above the irradiated area. Single dot exposure and current-limited regime were used for patterning.

The maximum area that can be patterned with the *Nova Nano lab 650 Dual Beam System* under high accuracy circumstances is limited to 4096 (X direction) by 3816 pixels (Y direction) [10, 20].

In order to control the focused electron beam, a streamfile was produced with *Matlab*. This file contained the coordinates of all pixels and wrote in an area ranging from 0 to 4095 pixels for the X coordinates, and 280 to 3816 pixels for the Y coordinates [10].

The pattern magnification of 15625 x was used to create the patterns. In this case 1 pixel equals 2 nm. The area of one stream file, for a pattern containing 35 by 35 pillars (also called an array), is approximately 5.8 µm by 5.8 µm.

Specific settings were fixed to produce the pattern (*table 4*). The used pattern strategy was to focus the stationary electron beam on a point, resulting in a single dot exposure, which grows the pillar in a vertical position along the beam axis [16, 20]. This was done for every point in the stream file. The points in the streamfile were placed exactly 170 nm next to each other. Therefore, the interpillar distance could be precisely controlled.

**Table 4: Pattern settings used to produce pillars with diameter 80 nm, height 190 nm and interpillar distance of 170 nm by EBID.**

| Pattern settings | | | | | | | | | | |
|---|---|---|---|---|---|---|---|---|---|---|
| $V_{beam}$ **[kV]** | $I_{beam}$ [nA] | **Array** [pillars] | $t_{dwell}$ [ms] | **Repeats** [-] | **Passes** [-] | $t_{refresh}$ [µs] | $t_{total}$ [min:s] | $T_{GIS}$ [°C] | **Deflection** [-] | **Stage shift** centre-to-centre stream file [µm] |
| **17.8** | 0.60 | 35x35 (5.8x5.8 µm$^2$) | 3 | 1 | 100 | 3 | 06:08 | 39.01 | 64 | 6.09 |

In order to create one patterned surface with an area of 40 x 40 µm$^2$ in the middle of the sample, 49 stream files were stitched together. When stitching multiple stream files next to each other, the stream files were written by a serpentine writing strategy (*figure 4*). Between every stream file a manual stage shift was performed to prevent overlapping and this was also checked by using the snapshot function.

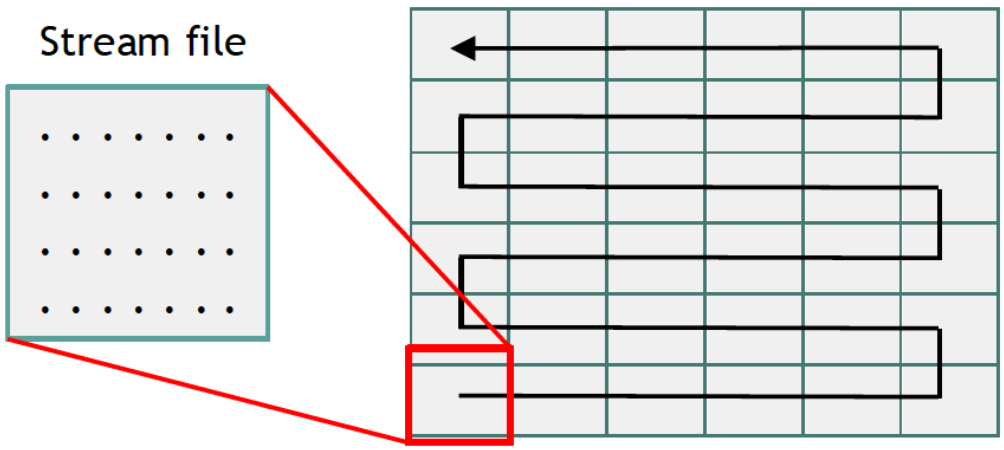


**Figure 4: Serpentine strategy: step and repeat process for increasing the total area of patterning [10].**

The dimensions of the pillars were checked using the measurement tools of SEM after patterning of the first and last stream file. Refocusing was done at the beginning of every row and after patterning the fourth stream file in each row.

To create the platinum-carbon control surfaces (Pt-C control), the precursor gas was let in to the chamber and reached a stable pressure of 2.75 - 2.81 $10^{-006}$ mbar. The magnification was set to 2000 x, the voltage was 17.8 kV, the current was 0.60 nA, contrast was between 65.0 - 67.1 and brightness of 46.1 - 46.2.
By SEM imaging an area of 63.25 x 63.25 $\mu m^2$ for 15 minutes with a scanning dwell time of 300 ns, a thin layer of platinum-carbon EBID deposition was created.

### 2.1.4 Pattern characterization by SEM

After patterning the surfaces, the precursor gas was pumped out and left overnight until the pressure inside the chamber reached 8.58 $10^{-007}$ mbar.

Sixty different random pillars per area of 40 x 40 $\mu m^2$ were measured. From those data points the mean height, diameter and interpillar distance were determined in combination with the standard deviation. The interpillar distance was precisely controlled beforehand by the streamfile. Nevertheless, it was checked if this was indeed the case.

A horizontal focal width (HFW) of 512 nm was used for all the measurements. The voltage was 5 kV, the current was 0.40 nA, the brightness ranged between 43.3 and 47.0 and the contrast between 64.5 and 68.0. The working distance was approximately 5 mm.

The diameter was determined by the width of the base and the tip of the pillar, resulting in a base and tip diameter. This was measured with the SEM image tool “line” while the tilt angle was 35 degrees and the setting option “horizontal direction”, “automatic tilt type” and “surface tilt correction” were selected.

The height of the pillar was also measured under an angle of 35 degrees by using the image tool “line”, option “vertical direction”, “automatic tilt type” and “cross-section tilt correction” as a perpendicular line from base centre till top of the pillar.

The centre-to-centre distance of two neighbouring nanopillar tips determined the interpillar distance. This was measured with the SEM image tool “line” while the tilt angle was 0 degrees, automatic tilt and tilt correction were set to “none”.

## 2.2 Bacterial cultures

The Gram-negative rod-shaped bacterium, *Escherichia coli,* is a widely investigated microorganism and is one of the pathogens present at the peri-implant infection site. The Gram-positive, cluster-forming coccal-shaped bacterium, *S. aureus*, is one of the most abundant microorganisms present at the peri-implant infection site [1-3].

For this reason, *S. aureus* together with *E. coli* are used to assess the bactericidal properties of the pattern.

Before incubating the samples with *E. coli* and *S. aureus*, the samples were soaked with 70% ethanol for 3 minutes and sterilized with UV light for 20 minutes. The sterilized samples were dried and placed in 24-well cell culture plates.

### 2.2.1 *E. coli* growth conditions and incubation

The following procedure was used to grow and incubate the samples with *E. coli,* K-12 strain (*figure 5*)*:*
The medium Lysogeny-broth (LB) was used to grow and cultivate *E. coli.* This liquid medium was produced from 1% bacto-tryptone, 0.5% bacto-yeast extract and 1% NaCl in demineralized water. A liquid and solid version of LB was used. The solid LB was made by adding 15 grams of bacto agar per liter of liquid LB. Both liquid and solid LB (agar) was autoclaved at 121 °C for 4 hours.

After pouring plates from the heated solid LB, a loop of bacteria stock was streaked onto the LB agar plate and incubated for 24 hours at 37 °C. When preparing a pre-culture, a single homogeneous colony was picked up from the LB agar plate and added to liquid LB. This solution of *E. coli* bacteria and liquid LB was continuously shaken at 140 RPM and 37 °C for 22 hours.

After 22 hours, the optical density (OD) of the culture was measured by using *WPA Biowave II* absorption spectroscopy at a wavelength of 600 nm ($OD_{600}$). The culture was diluted in liquid LB to obtain a bacterial cell suspension with $OD_{600}$ = 1, which means this suspension contains 15 x $10^7$ *E. coli* CFUs per 100 µL. This was confirmed by counting the amount of *E. coli* bacteria on incubated LB agar plates.

0.5 mL of liquid LB was added to the wells to enhance the wetting. Next, the *E. coli* bacterial suspension was diluted in liquid LB to $OD_{600}$ = 0.1.
In addition, 0.5 ml of this dilution was added to each well. This resulted in a bacterial cell suspension with $OD_{600}$ = 0.05.
The 24-well plate, including the bacterial cell suspensions, was mixed at 100 RPM for 5 min and incubated at 37 °C for 18 hours.

### 2.2.2 *S. aureus* growth conditions and incubation

The following procedure was used to grow and incubate the samples with *S. aureus,* RN0450 strain (*figure 5*)*:*
The medium Brain Hearth Infusion broth (BHI) was used to grow and cultivate *S. aureus.* This liquid medium was produced from 37 grams BHI powder (*Fluka Analytical, BCBN2163V)* in 1L of distilled water. A liquid and solid version of BHI was used. The solid BHI was made by adding 52 grams of BHI agar (*Fluka Analytical, BCBM2747V)* in 1L of distilled water. Both liquid and solid BHI (agar) were autoclaved at 121 °C for 4 hours.

After pouring plates from the heated solid BHI, a loop of bacteria stock was streaked onto the BHI agar plate and incubated for 24 hours at 37 °C. When preparing the pre-cultures, a single homogeneous colony was picked up from the BHI agar plate and added to liquid BHI. This solution of *S. aureus* bacteria and liquid BHI was continuously shaken at 140 RPM and 37 °C for 22 hours.

After 22 hours, the optical density (OD) of the overnight culture was measured by using *WPA Biowave II* absorption spectroscopy at a wavelength of 600 nm ($OD_{600}$). The culture was diluted in liquid BHI to obtain a bacterial cell suspension with $OD_{600}$ = 1, which means this suspension contains 7 x $10^7$ *S. aureus* CFUs per 100 µL. This was confirmed by counting the amount of *S. aureus* bacteria on incubated BHI agar plates.

0.5 mL of liquid BHI was added to the wells to enhance the wetting. Next, the *S. aureus* bacterial cell suspension was diluted in liquid BHI to $OD_{600}$ = 0.1.
In addition, 0.5 ml of this dilution was added to each well. This resulted in a bacterial cell suspension with $OD_{600}$ = 0.05. The 24-well plate, including the bacterial cell suspensions, was mixed at 100 RPM for 5 min and incubated at 37 °C for 18 hours.

### 2.2.3 Sample preparations

After 18 hours of incubation, the samples were taken out of the wells and placed in empty wells. The bacterial cell suspensions were removed from the wells and the ODs were measured again with the *WPA Biowave II* absorption spectroscopy.
In every well that contained a sample, 1 ml of 0.01 M phosphate-buffered saline (PBS) was added and shaken at 50 RPM for 5 minutes. The isotonic PBS helps to clean the bacterial cultures without damaging the cells.

Afterwards the PBS was removed and 1 ml of fixation solution was added to each sample-containing well in order to preserve the shape of the adherent bacteria and was left for 2 hours in the fridge at 4 °C. This fixation solution consisted out of 4% formaldehyde and 1% glutaraldehyde in 10 mM phosphate buffer.

After the 2-hour waiting period the samples were washed by adding 1 ml of MiliQ water to every sample-containing well and shaken at 50 RPM for 10 minutes.

Once the MiliQ water was removed, a series of ethanol washings was performed which dehydrated the bacteria on the samples:
(1) Adding 1 ml of 50% ethanol to the wells and shaken at 50 RPM for 15 minutes
(2) 70% ethanol at 50 RPM for 20 minutes, and
(3) 96% ethanol at 50 RPM for 20 minutes.

Lastly, 1 ml of the chemical drying agent hexamethyldisilazane (*Sigma-Aldrich, Missouri*) was added to each sample and left for 30 minutes in the flow cabinet. After 30 minutes this chemical drying agent was removed from the samples and air-dried for approximately 18 hours. Afterwards the samples were gold sputtered for 18 seconds in order to contain a thin layer of gold, which enhances the conductivity necessary for SEM imaging.

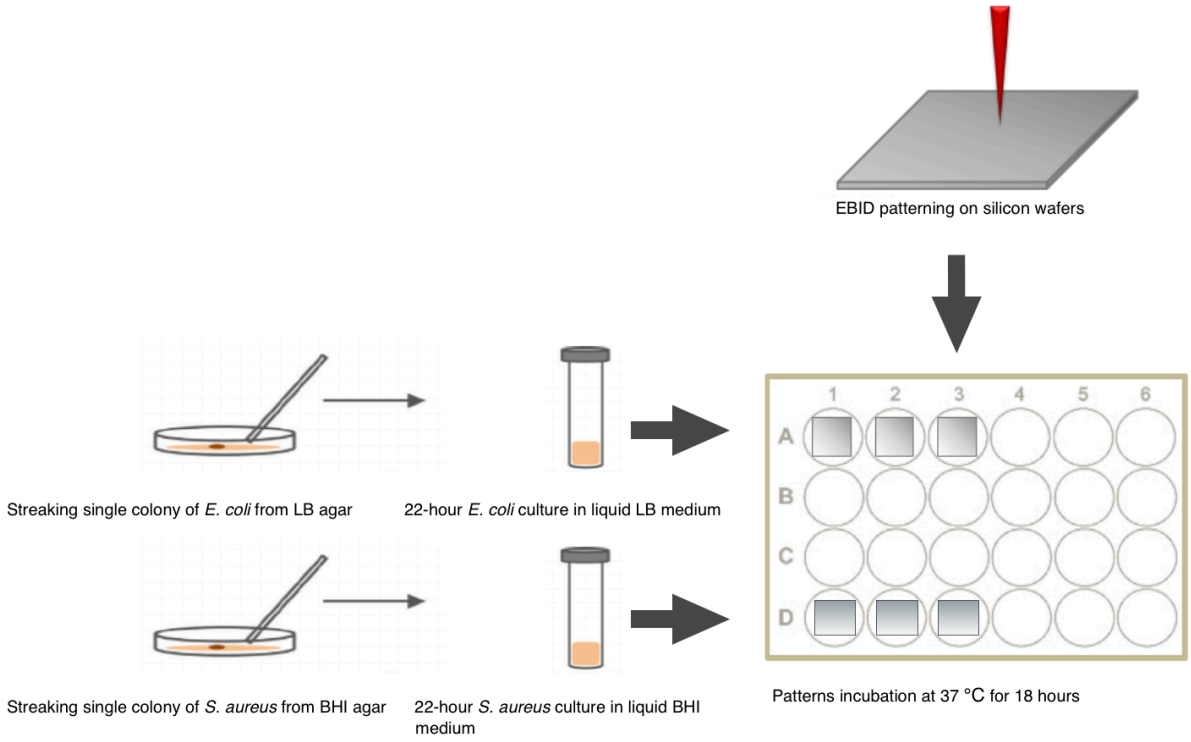


**Figure 5: Overview experimental set-up**

### 2.2.4 Analysis of bacterial morphology and bactericidal efficacy

After gold sputtering was performed on the samples, they were placed in the *Nova Nano Lab 650 Dual Beam system (FEI company).*
The working distance was approximately 5 mm. In order to analyse the bacteria on the samples, SEM was used with a beam acceleration voltage of 5 kV and a beam current of 0.4 nA. The brightness ranged between 43.3 and 47.0 and the contrast between 64.5 and 68.0.

From the obtained SEM images the morphology and amount of damaged bacteria were determined on specific areas. The red area is the patterned surface (grey squares) and the surface closely to the patterns. The green areas are the Si control surfaces, 1 mm away from the red (patterned) area (*figure 6*). For the Pt-C control surfaces only the green areas were inspected, since these samples were non-patterned.

The morphology included shape, diameter, cell length/major axis and width/minor axis and was determined by using the SEM measuring tools.

In order to determine the bactericidal efficacy, the bacterial density was first calculated.
The bacterial density was determined by estimating the amount of total bacteria (live and dead) on the different areas (specific surface bacterial density). The estimation was done by manually counting the bacteria in the different areas (*figure 6*).

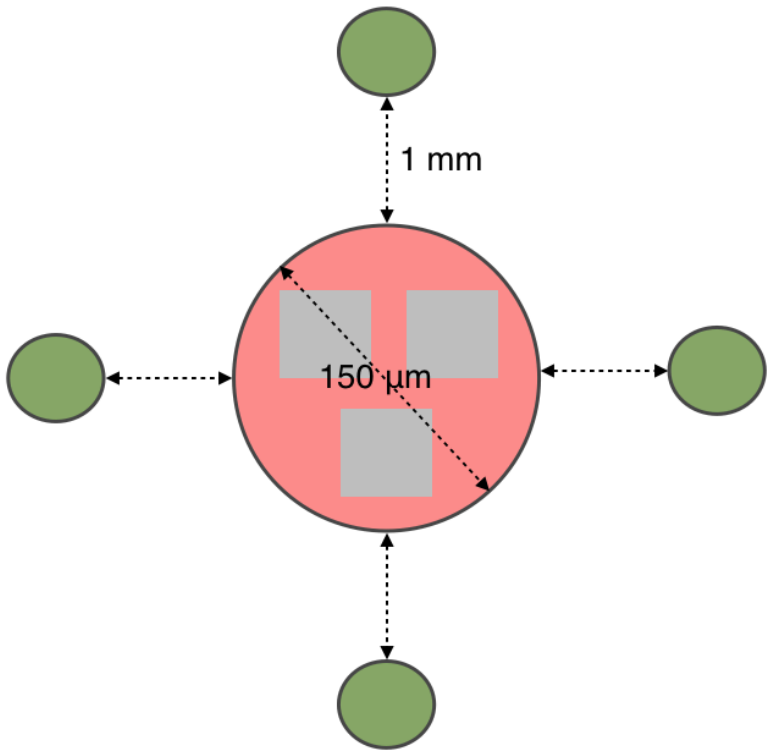


**Figure 6: Inspected areas (on one sample) for analysing morphology, bacterial density and bactericidal efficacy: red area is (close to) patterned surface, green areas are far from patterned area (1 mm distance)**

The amount of damaged bacterial cells was also counted in the same manner. The bacterium was considered to be damaged if wrinkling and deformation occurred on the cell surface (*figure 7*).

The bactericidal efficacy of the patterned and control surfaces was assessed by the damaged-to-total bacteria ratio. This was expressed as the percentage of damaged bacterial cells relative to the specific surface bacterial density.

A statistical analysis was performed with *SPSS* statistical analysis software in order to observe significant differences between the control surfaces and patterned surfaces for each bacterial species and between the two bacterial species. This was done by using an analysis of variance (one-way ANOVA or Kruskal-Wallis test) and by pair-wise comparisons of the different surfaces with Bonferroni post-hoc test.
The variation in pillar dimensions within all nine patterns was also observed by using the explore function of *SPSS* statistical analysis software.

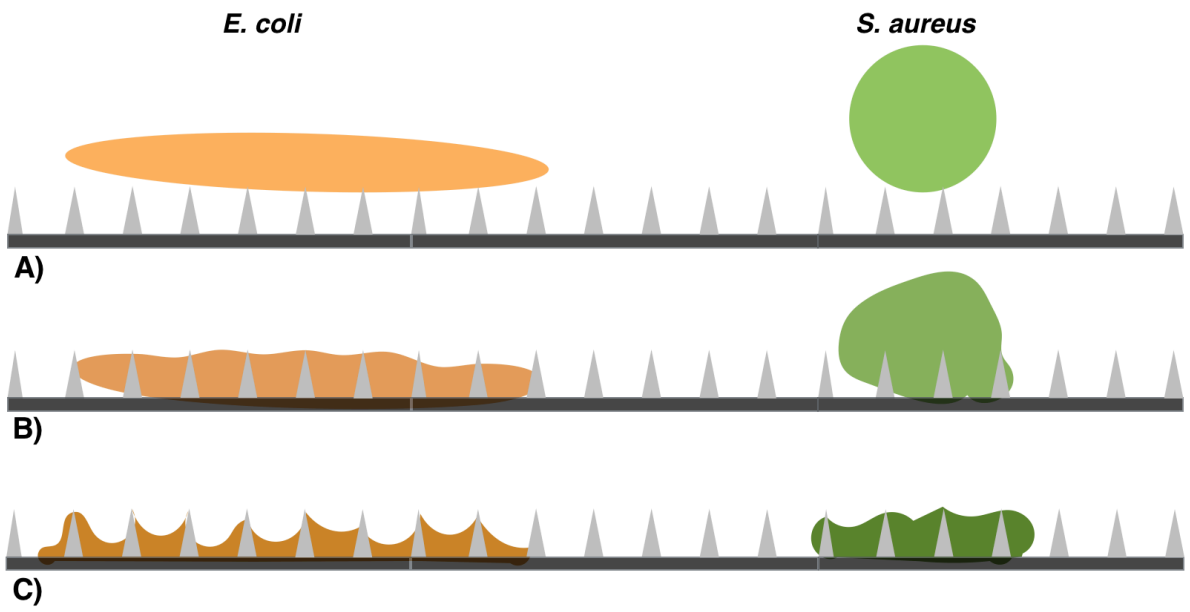


**Figure 7: Schematics of interaction of *E. coli* and *S. aureus* with nanopillars. A) Healthy bacterial cells on pattern B) Deformed bacterial cells on pattern C) Severely deformed bacterial cells on pattern**

# 3 Results

## 3.1 Fabrication and characterization of pattern with EBID and SEM

The pattern with specified dimensions was produced with EBID (*figure 12*). Two samples with each 3 patterned surfaces were created. In total there were 6 patterned surfaces of each 42 by 42 $\mu m^2$ produced (for assessing the bactericidal efficacy).

The shape of the pillars was similar to a droplet-shaped structure with a different base- and tip diameter. The base diameter was 75 ± 5 nm (mean ± standard deviation) and the tip diameter was 21 ± 3 nm. The height of the pillars was 186 ± 8 nm. The interpillar distance was 172 ± 4 nm. This led to a pillar density of 36 pillars per $\mu m^2$ (*table 5*).

**Table 5: Results nanopillar dimensions: mean diameter, height and interpillar distance including standard deviation and pillar density**

| Topography | Diameter [nm] | Height [nm] | Interpillar distance [nm] | Pillar density [n/ $\mu m^2$] |
|---|---|---|---|---|
| Nanopillars | 75 ± 5 nm | 186 ± 8 nm | 172 ± 4 nm | 36 |

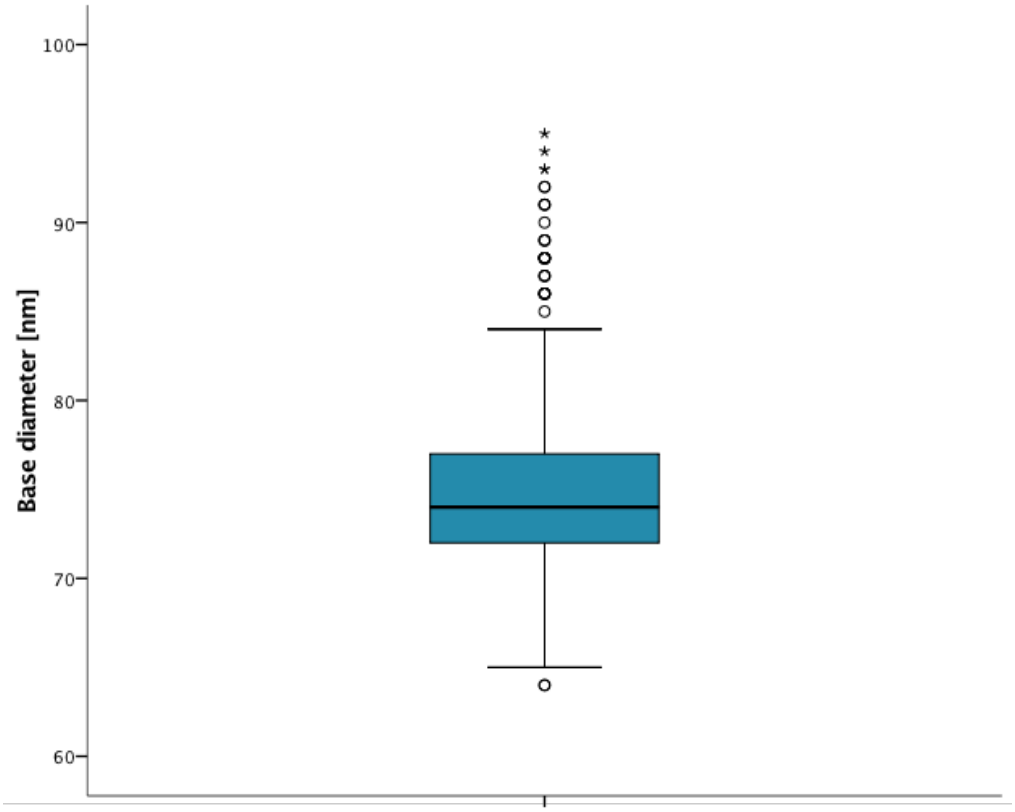


Figure 8: Boxplot of pillar base diameter, showing median, maximum- and minimum values (whiskers) and outliers (°, *) of all patterns

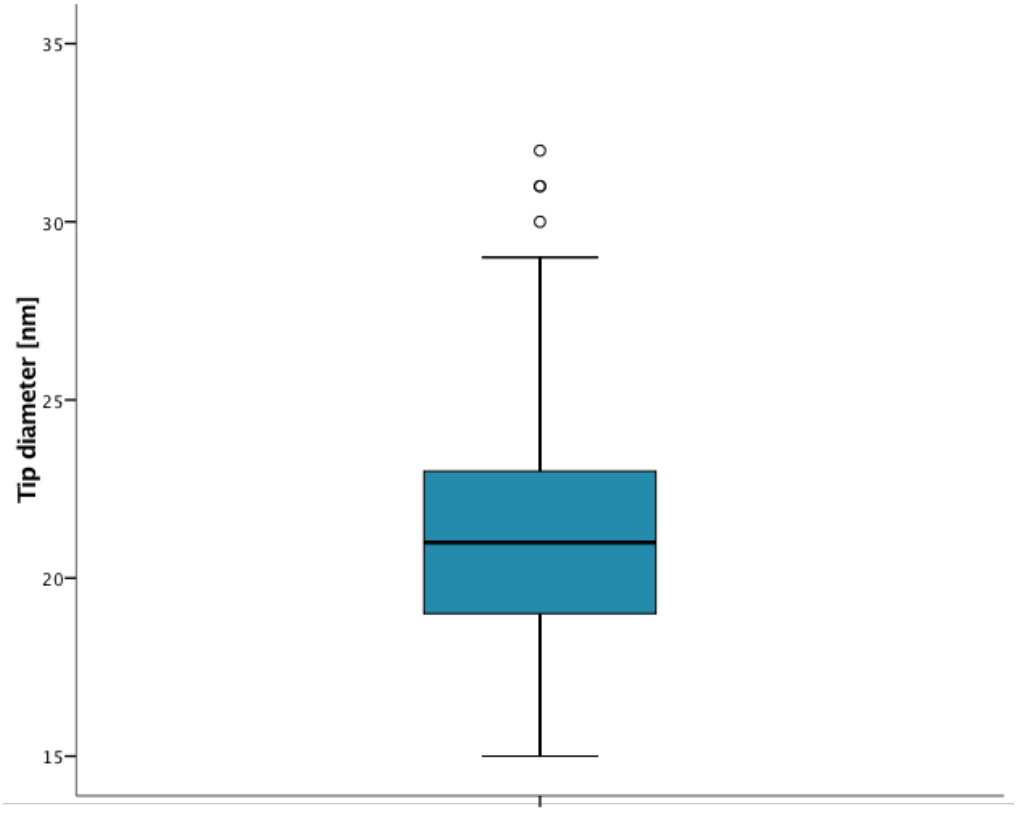


Figure 9: Boxplot of pillar tip diameter, showing median, maximum- and minimum values (whiskers) and outliers (°) of all patterns

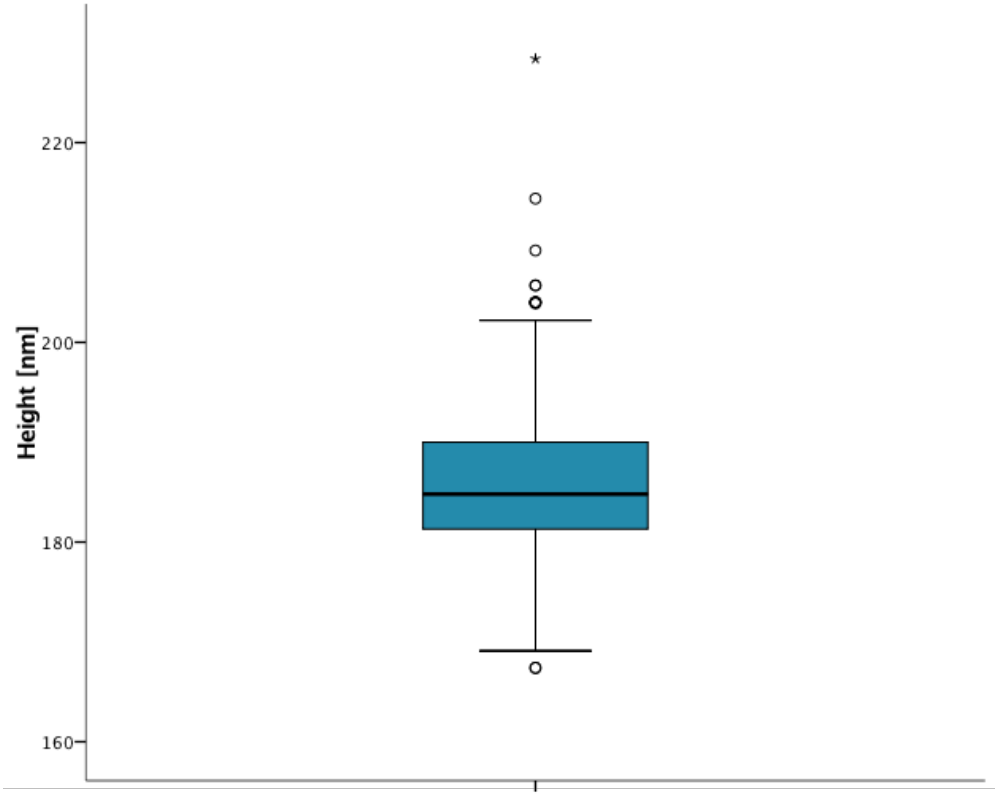


Figure 10: Boxplot of pillar height, showing median, maximum- and minimum values (whiskers) and outliers (°) of all patterns

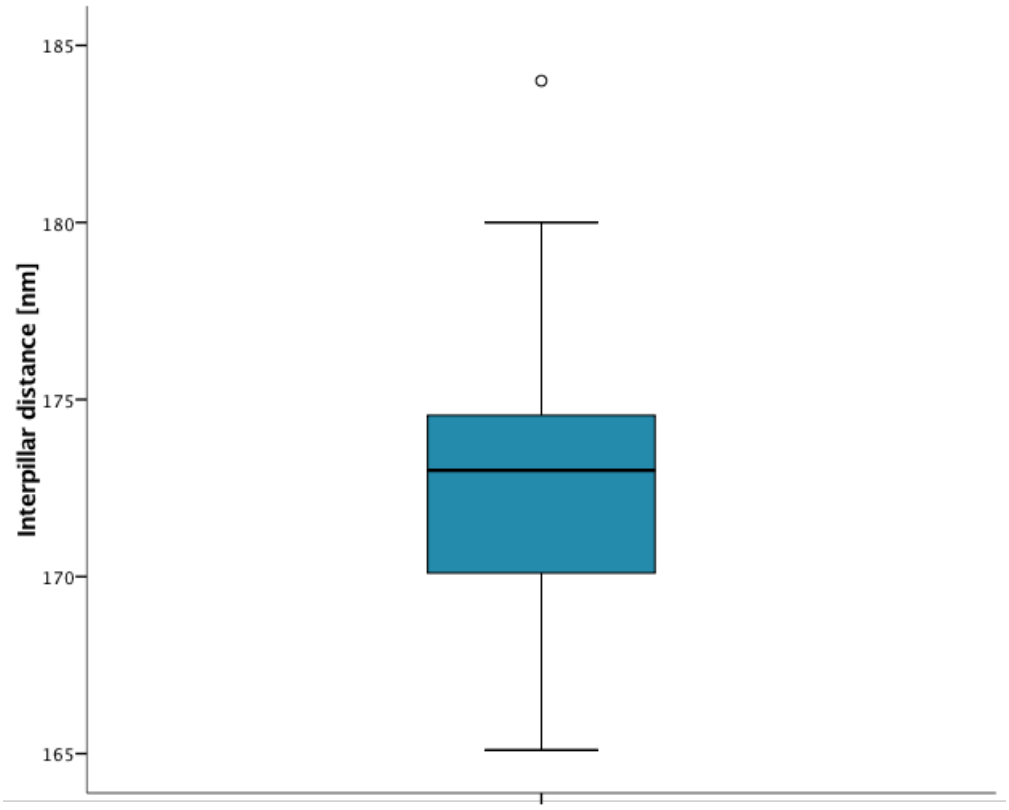


Figure 11: Boxplot of interpillar distance, showing median, maximum- and minimum values (whiskers) and outliers (°) of all patterns

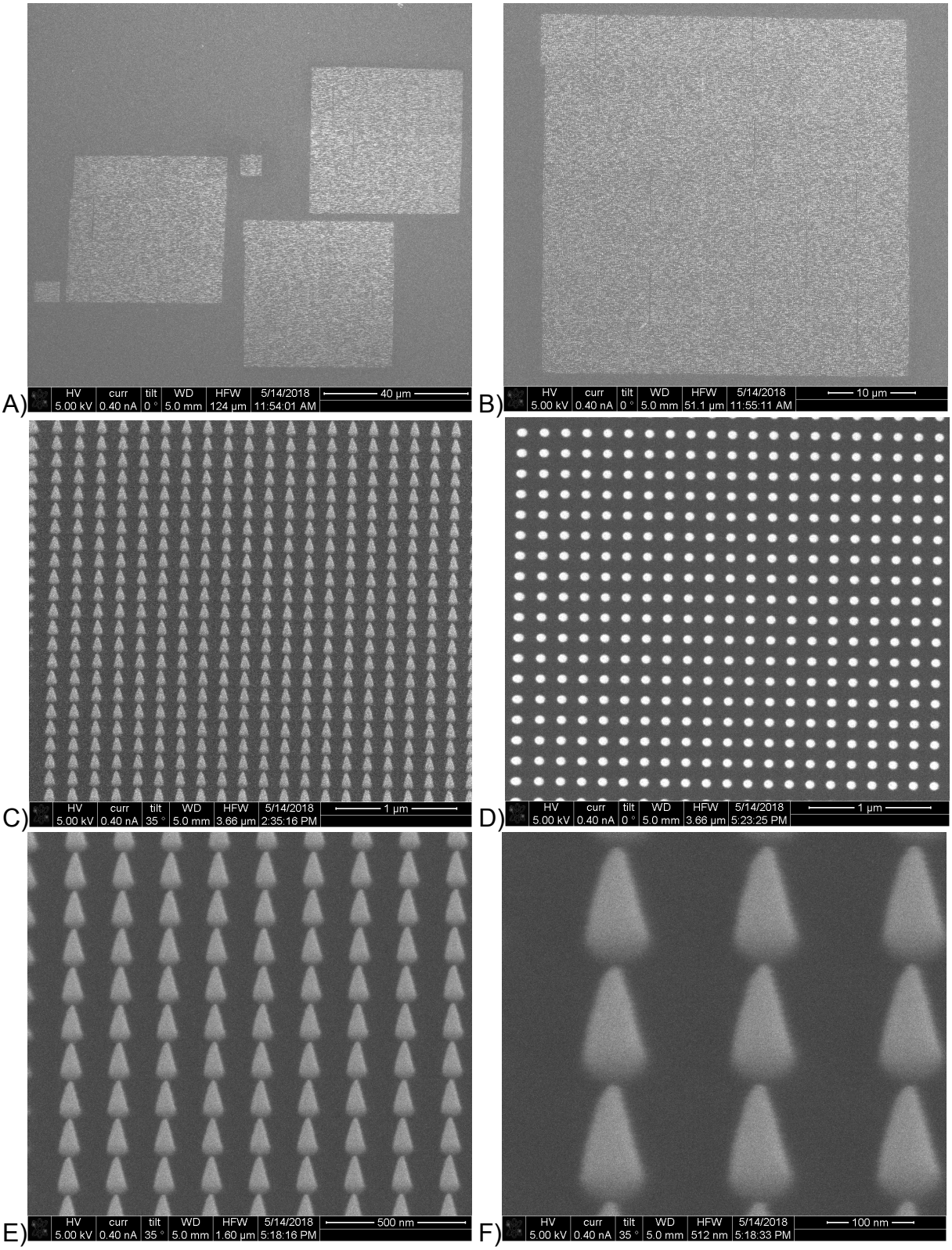


**Figure 12: SEM images of patterns containing nanopillars. A) Overview image of three patterned surfaces, each pattern occupying an area of 42 x 42 µm$^2$ and two smaller test patterns of 6 x 6 µm$^2$ (scale bar 40 µm) B) Overview image of one pattern of 42 x 42 µm$^2$ (scale bar 10 µm) C) Tilted image of pattern (scale bar 1 µm) D) Top view image of pattern (scale bar 1 µm) E) Tilted image of pattern (scale bar 500 nm) F) Tilted image of pattern (scale bar 100 nm)**

## 3.2 Bacterial morphology and bactericidal efficacy

### 3.2.1 Response of *E. coli* cells on patterned sample 1 and control surfaces

The *E. coli* cells on both the Si control surface as the Pt-C control surface seem to exhibit rod-shaped cell morphology without significant damages (*figure 13-14*). The average percentage of damaged bacterial cells on the Si control surface was 8.0 ± 6.4% (mean ± standard deviation). The average cell length of *E. coli* on the Si control surface was 2.61 ± 0.68 µm and the average cell width was 807.7 ± 106.6 nm (*table 6*).
The Pt-C control surface had an average percentage of damaged bacterial cells of 1.6 ± 2.7% and was used to assess the bactericidal efficacy of the surface chemistry (*table 7*).

Each SEM image of the incubated patterns shows that most *E. coli* cells are completely deformed and are not recognizable as *E. coli* compared to the *E. coli* cells on the Si control surface on the same sample (sample 1) and the Pt-C control surface (*figure 15*).
There also seems to be a substantial amount of bacterial cell membranes left on the patterned surface in combination with possible extracellular polymeric substances (EPS) and bacterial cell contents. The percentage of damaged *E. coli* cells on the patterned surface was 96.9 ± 1.2% (*table 8*).

On the area closely to the patterned surface there also seemed to be damaged *E. coli* cells and cell membranes visible (*figure 16*). The damaged cells look much smaller in size than the cells on the Si control surface.

Unfortunately, because of these large cell deformations, the cell width and length of the bacterial cells on the patterned surface could not be determined.

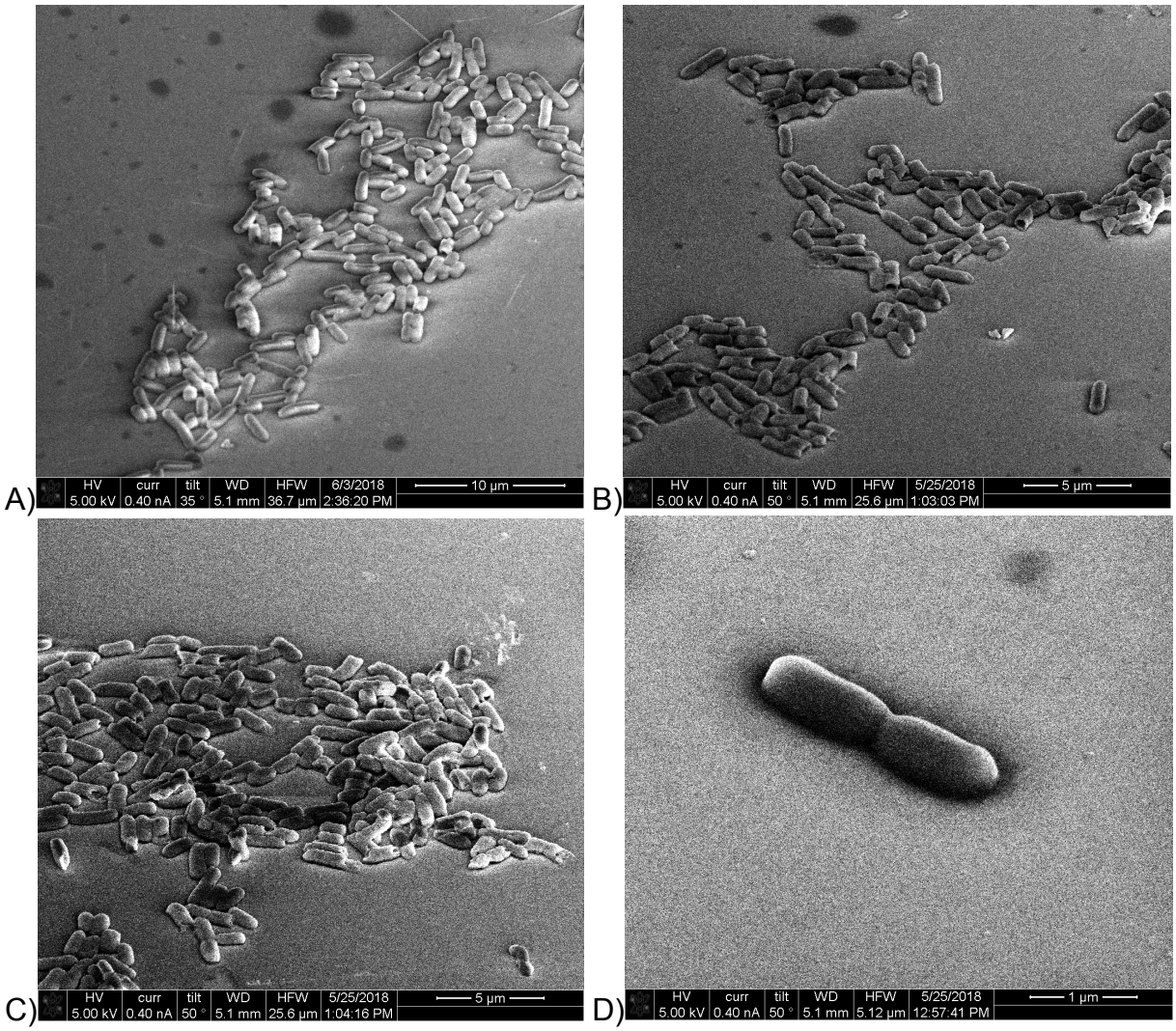


**Figure 13: SEM images of *E. coli* on Si control surfaces after 18 hours of incubation A) Tilted overview image bacteria-surface interaction of *E. coli* (scale bar 10 µm) B) Cluster of *E. coli* cells attached on Si control surface (scale bar 5 µm) C) Group of unharmed *E. coli* cells attached on Si control surface (scale bar 5 µm) D) Unharmed *E. coli* cell attached on Si control surface (scale bar 1 µm)**

**Table 6: Mean and standard deviation of cell width, cell length and percentage of damaged *E. coli* cells on Si control surface**

| Surface | Cell width [nm] | Cell length [µm] | Damaged *E. coli* cells [%] |
|---|---|---|---|
| **Si control** | 807.7 ± 106.6 | 2.61 ± 0.68 | 8.0 ± 6.4 |

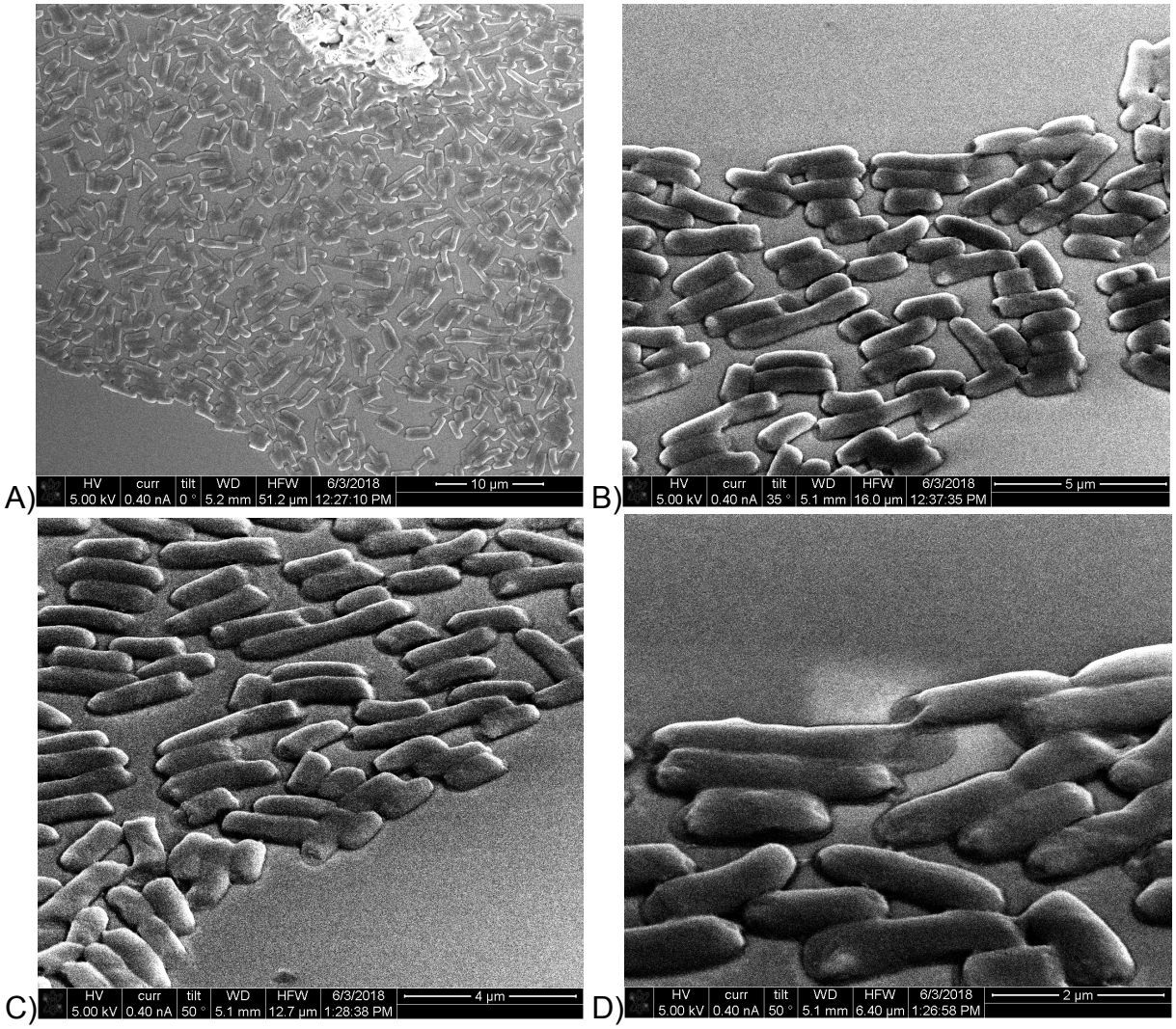


**Figure 14: SEM images of *E. coli* on Pt-C control surfaces after 18 hours of incubation A) Tilted overview image bacteria-surface interaction of *E. coli* (scale bar 10 µm) B) Group of *E. coli* cells attached on Pt-C control surface (scale bar 5 µm) C) Group of possibly dividing *E. coli* cells attached on Pt-C control surface (scale bar 4 µm) D) Unharmed *E. coli* cell with EPS attached on Pt-C control surface (scale bar 2 µm)**

**Table 7: Mean and standard deviation of damaged *E. coli* cells (%) on Pt-C control surface**

| Surface | Damaged *E. coli* cells [%] |
|---|---|
| **Pt-C control** | 1.6 ± 2.7 |

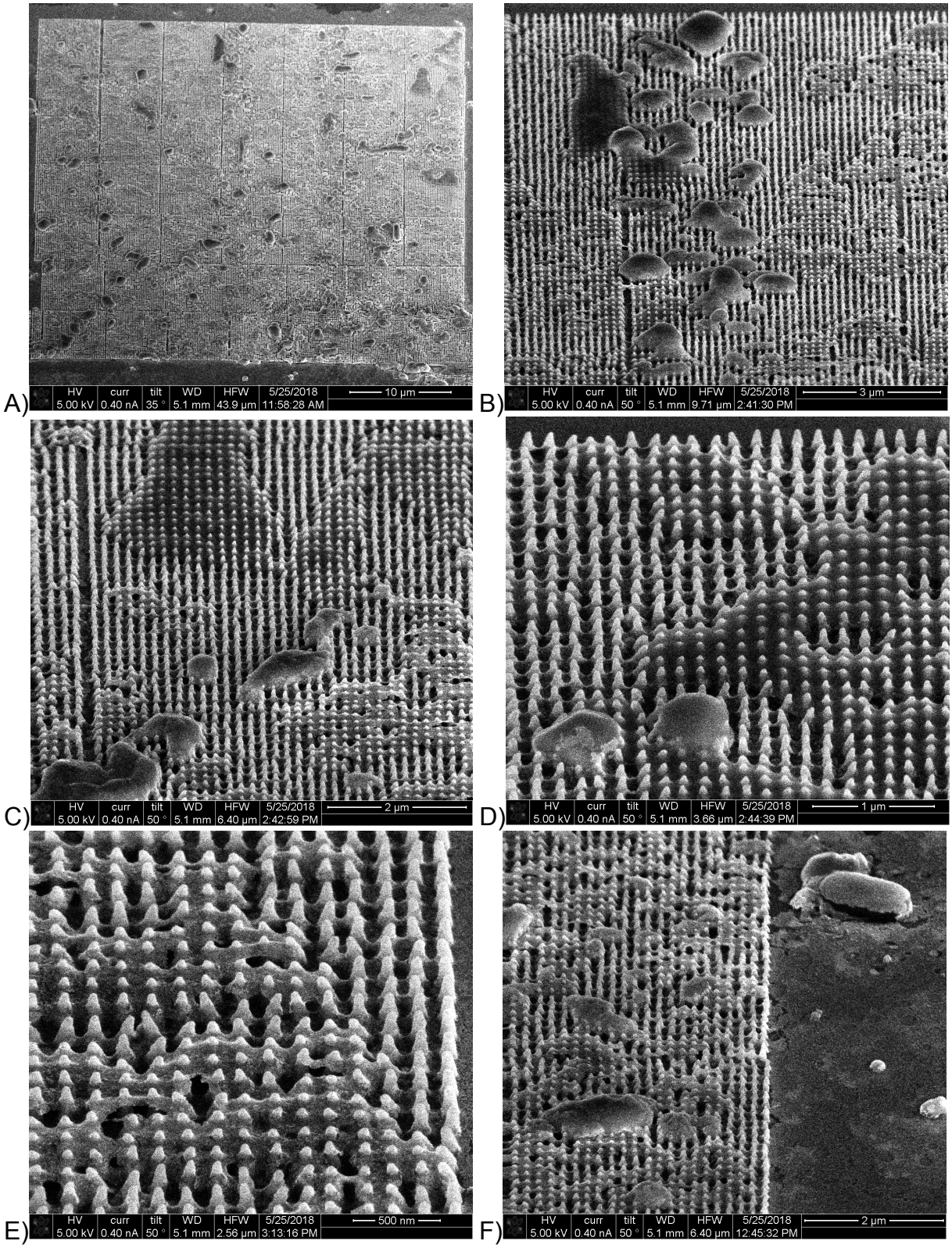


**Figure 15: SEM images of *E. coli* on patterned surface after 18 hours of incubation A) overview image bacteria-pattern interaction of *E. coli* (scale bar 10 µm) B) Deformed and damaged *E. coli* cells (scale bar 3 µm) C) Completely deformed *E. coli* cells (scale bar 2 µm) D) Deformed *E. coli* cells and possible left over bacterial cell membranes and EPS (scale bar 1 µm) E) Possible left over bacterial substances (scale bar 500 nm) F) Deformed *E. coli* cells on pattern and on area close to pattern**

Table 8: Mean and standard deviation of damaged *E. coli* cells (%) on patterned surface

| Surface | Damaged *E. coli* cells [%] |
|---|---|
| **Pattern** | 96.9 ± 1.2 |

A) 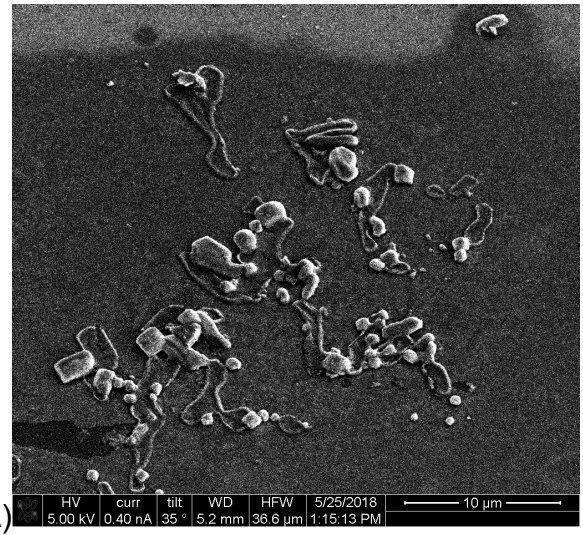


B) 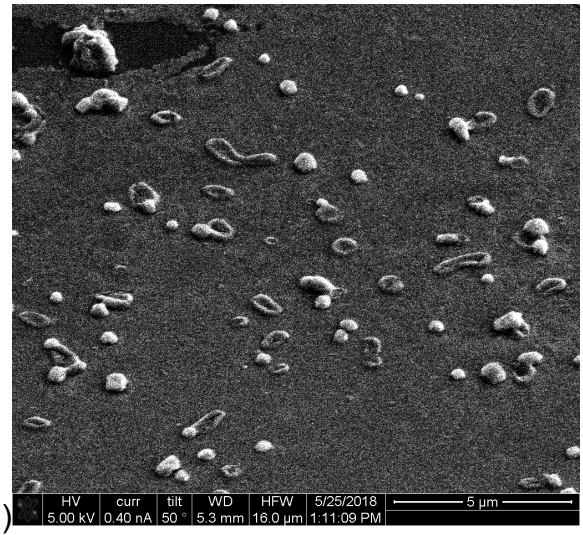


Figure 16: SEM images of *E. coli* on area close to patterned surface after 18 hours of incubation A) Deformed and possible left over *E. coli* cell membranes (scale bar 10 µm) B) Deformed and damaged *E. coli* cells on area close to patterned surface (scale bar 5 µm)

### 3.2.2 Response of *S. aureus* on patterned sample 2 and control surfaces

The *S. aureus* cells on both the Si control surfaces as the Pt-C control surfaces seem to exhibit coccal-shaped cell morphology without significant damages (*figure 17-18*). The average percentage of damaged bacterial cells on the Si control surfaces was 0%. The average diameter of *S. aureus* on the smooth surface was 789.9 ± 66.4 nm for the major axis and 710.5 ± 47.8 nm for the minor axis (*table 9*).
The Pt-C control surface had an average percentage of damaged bacterial cells of 2.6 ± 2.7% and was used to rule out surface-chemistry dependent bactericidal activity (*table 10*).

Each SEM image of the incubated patterns shows that most *S. aureus* cells are deformed compared to *S. aureus* cells on the Si control surfaces on the same sample (sample 2). Some cells show a squashed-like morphology (*figure 19-B, E*), while others remain some height (*figure 19-C, D, F*). It seemed as if over the whole patterned surface there were bacterial substances left (*figure 22*). The bacterial substances covered at least 2 pillars and up to 9 pillars of space.

A few bacteria seemed unharmed by the pillars (*figure 21*). In addition, bending of the pillars underneath the damaged bacterial cell was observed (*figure 21-22*).
Nevertheless, the pattern was able to damage 83.9 ± 22.8% of the *S. aureus* cells on the patterned surface (*table 11*).

The area closely to the patterned surface seemed to show no damaged bacterial cells (*figure 20*). However, there is a large cluster of *S. aureus* cells visible that most likely has been extensively covered with gold (*figure 20-A*).

Overall, the percentage damaged bacterial cells on the Si control surfaces was relatively low compared to the patterned surfaces for both *E. coli* and *S. aureus*. In addition, the damage that was seen on the patterned surfaces was more severe than on the control surfaces (*figure 23*).

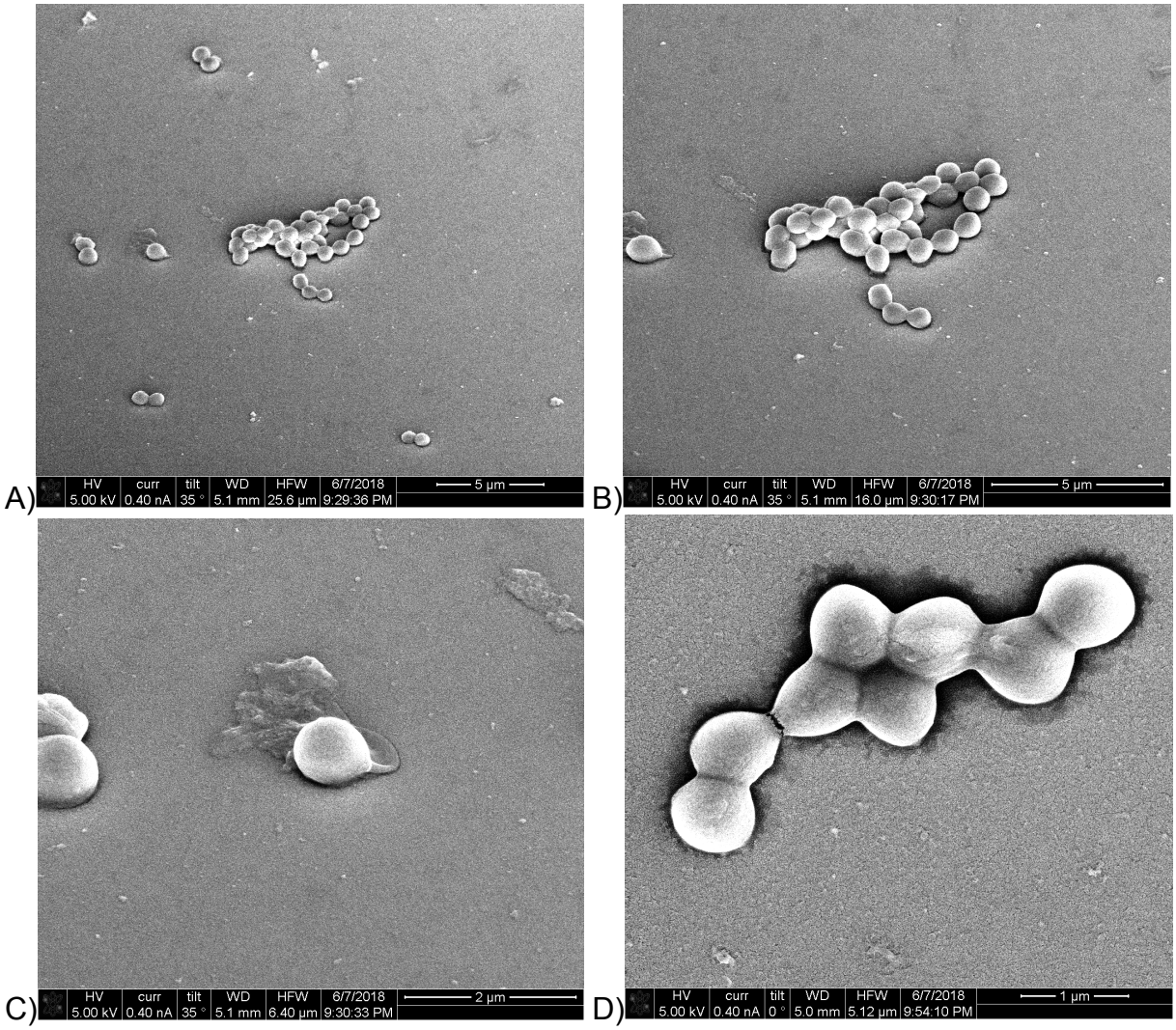


**Figure 17: SEM images of *S. aureus* on Si control surfaces after 18 hours of incubation A) Tilted overview image bacteria-surface interaction of *S. aureus* (scale bar 5 µm) B) Cluster of *S. aureus* cells attached on Si control surface (scale bar 5 µm) C) *S. aureus* cell with possible EPS attached on Si control surface (scale bar 2 µm) D) Unharmed *S. aureus* cells grouped together on Si control surface (scale bar 1 µm)**

**Table 9: Mean and standard deviation of cell diameter major axis, cell diameter minor axis and percentage of damaged *S. aureus* cells on Si control surface**

| Surface | Diameter major axis [nm] | Diameter minor axis [nm] | Damaged *S. aureus* cells [%] |
|---|---|---|---|
| **Si control** | 789.9 ± 66.4 | 710.5 ± 47.8 | 0 |

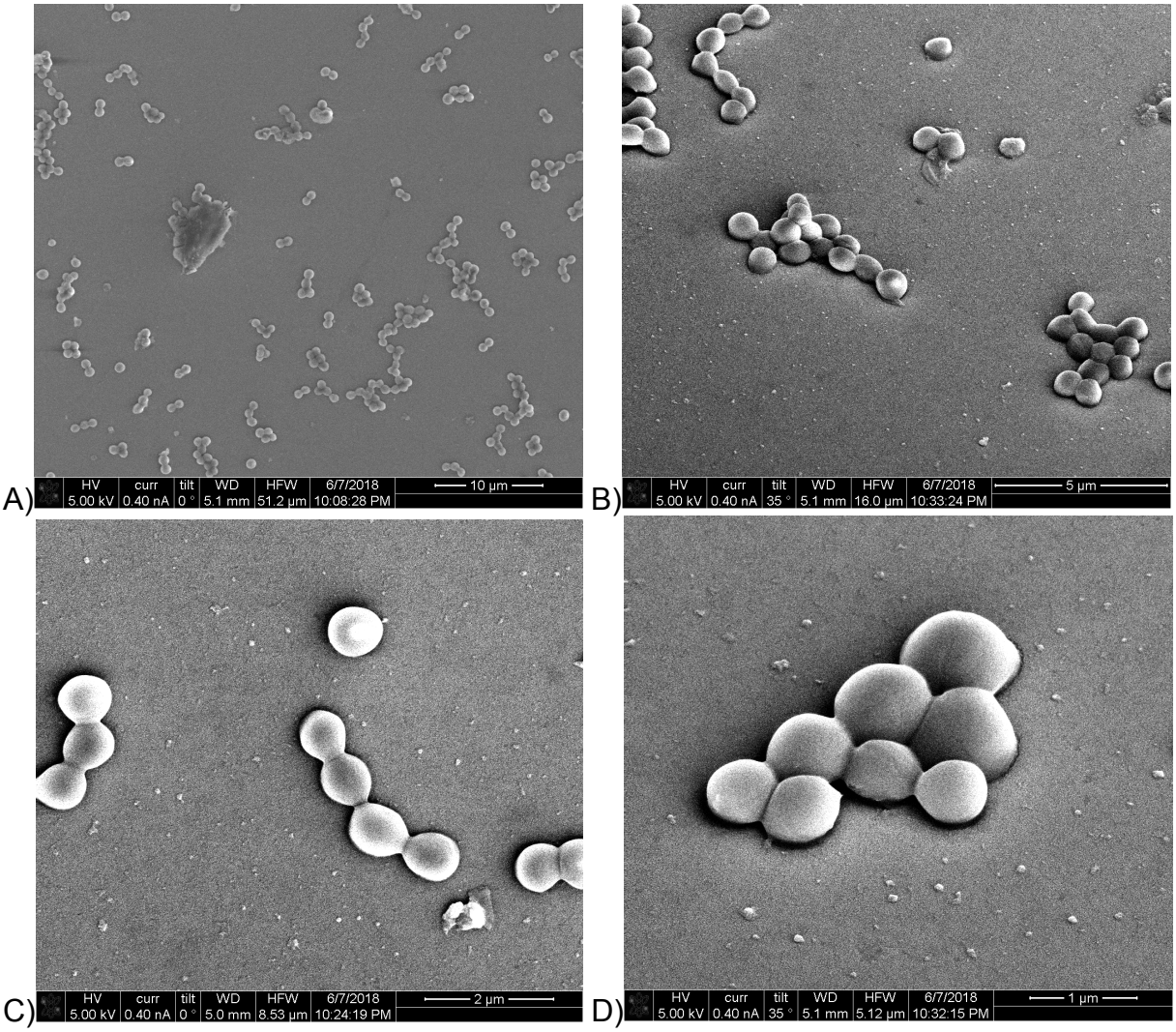


**Figure 18: SEM images of *S. aureus* on Pt-C control surfaces after 18 hours of incubation A) Overview image bacteria-surface interaction of *S. aureus* (scale bar 10 µm) B) Groups of *S. aureus* cells attached on Pt-C control surface (scale bar 5 µm) C) Small groups of *S. aureus* cells attached on Pt-C control surface (scale bar 2 µm) D) Group of unharmed *S. aureus* cells attached on Pt-C control surface (scale bar 1 µm)**

**Table 10: Mean and standard deviation of damaged *S. aureus* cells (%) on Pt-C control surface**

| Surface | Damaged *S. aureus* cells [%] |
|---|---|
| **Platinum-C control** | 2.6 ± 2.7 |

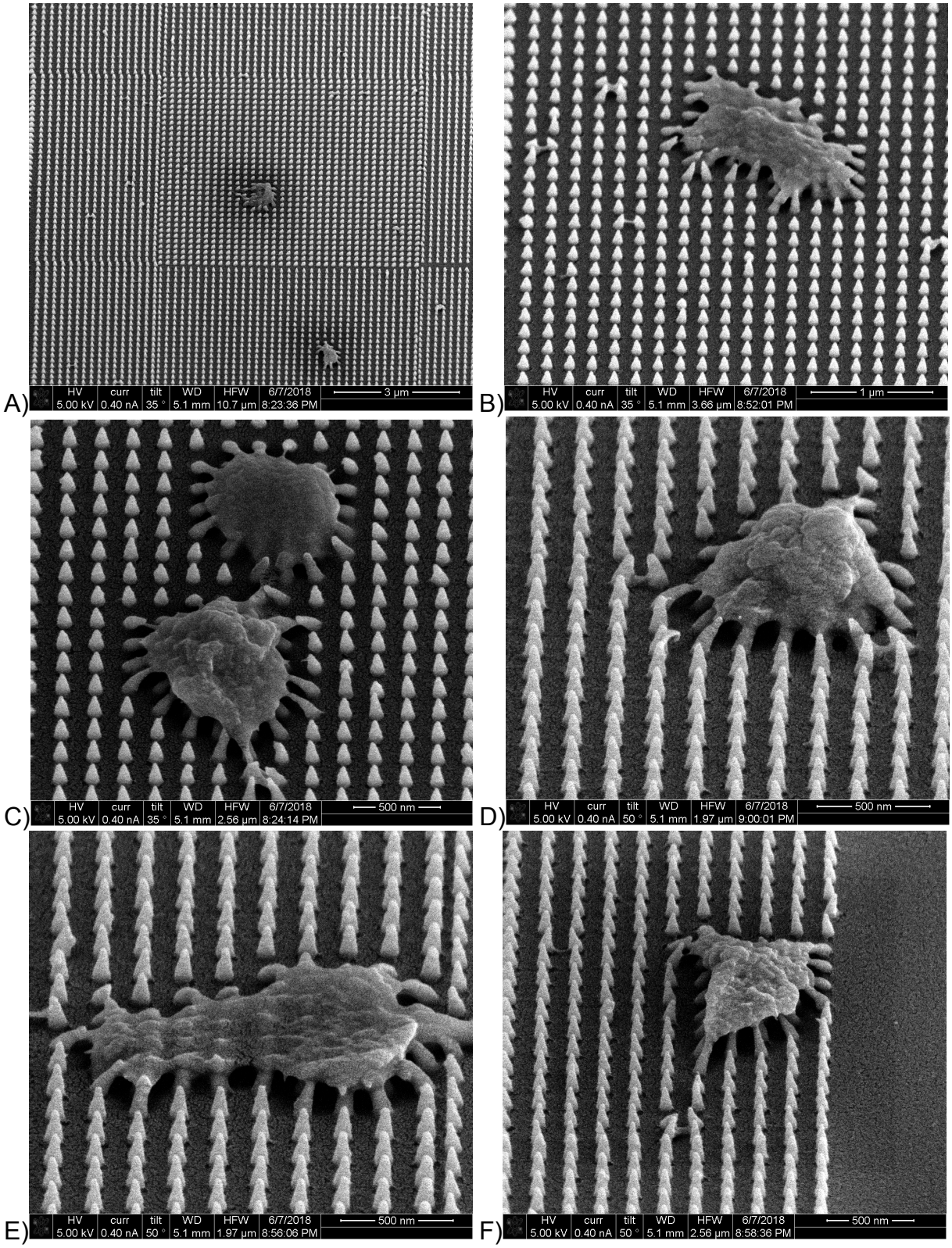


**Figure 19: SEM images of *S. aureus* on patterned surface after 18 hours of incubation A) Overview image bacteria-pattern interaction of *S. aureus* (scale bar 3 µm) B) Deformed *S. aureus* cell (scale bar 1 µm) C) Two deformed *S. aureus* cells (scale bar 500 nm) D) Deformed *S. aureus* cell pulling on pillars (scale bar 500 nm) E) Deformed and flattened *S. aureus* cell (scale bar 500 nm) F) Deformed *S. aureus* cells on pattern**

Table 11: Mean and standard deviation of damaged *S. aureus* cells (%) on patterned surface

| Surface | Damaged *S. aureus* cells [%] |
|---|---|
| **Pattern** | 83.9 ± 22.8 |

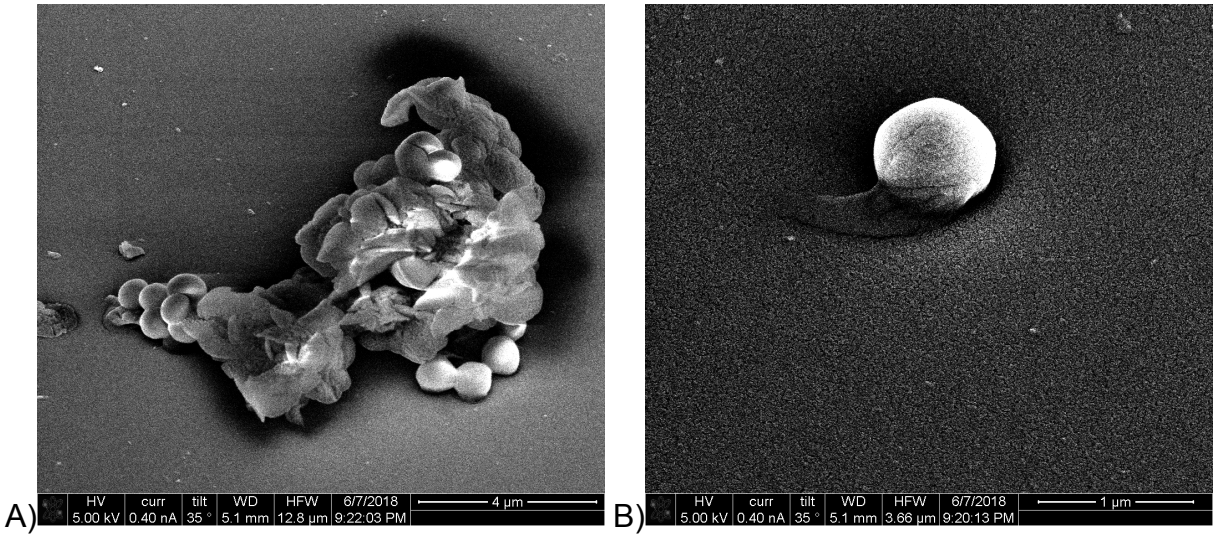


Figure 20: SEM images of *S. aureus* on area close to patterned surface after 18 hours of incubation A) Large cluster of *S. aureus* cells packed with gold particles (scale bar 4 µm) B) *S. aureus* cell with possible EPS on area close to patterned surface (scale bar 1 µm)

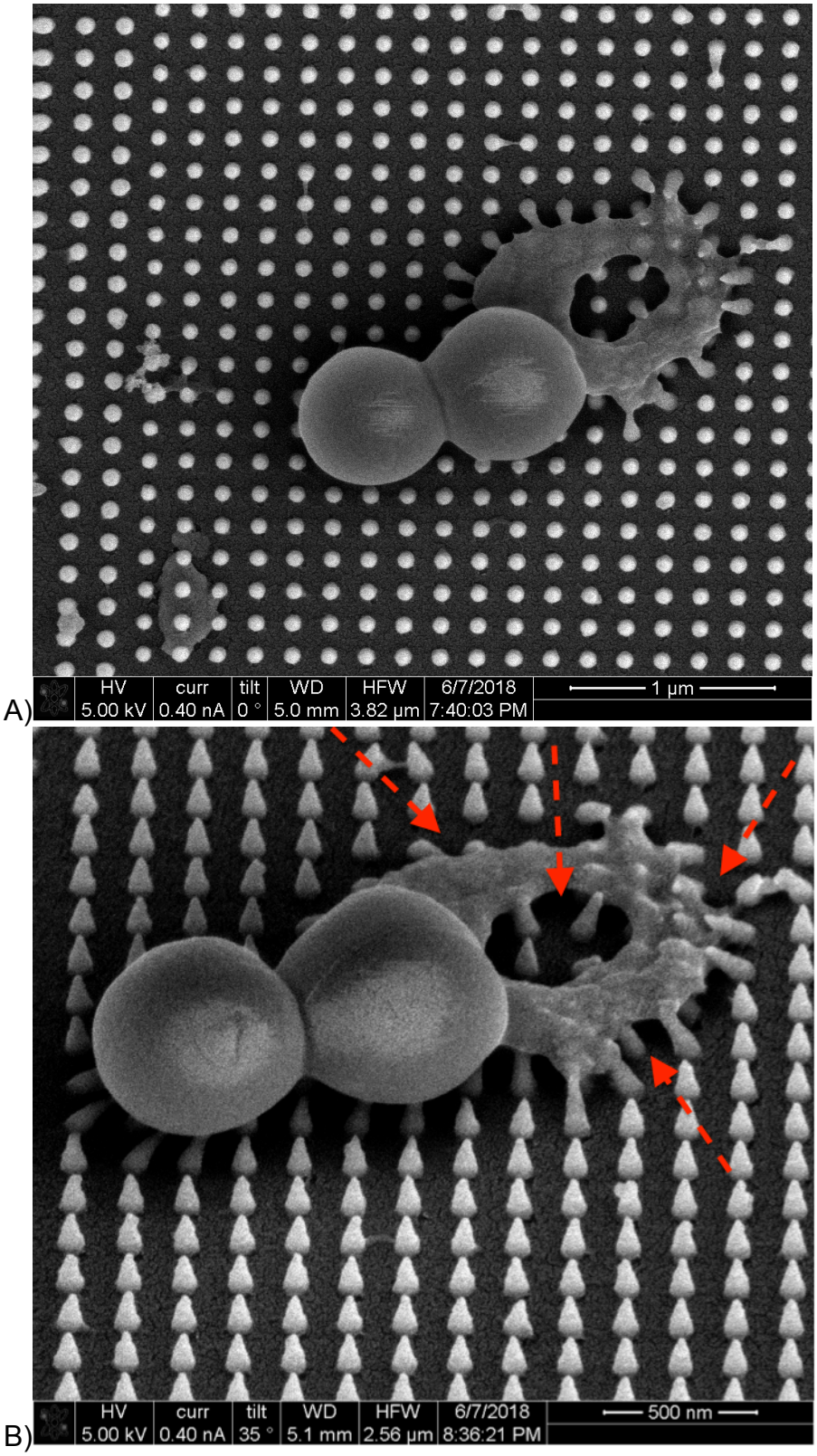


**Figure 21: SEM images of *S. aureus* cells on patterned surface A) Top view of *S. aureus* cells: two undamaged cells, one damaged cell that bends the pillars underneath and some bacterial substances found on the surface (scale bar 1 µm) B) Tilted image of three bacterial cells that bend the pillars underneath, the pillars underneath the damaged cell contents exhibit different directions (arrows) indicating possible migration attempts of *S. aureus* (scale bar 500 nm).**

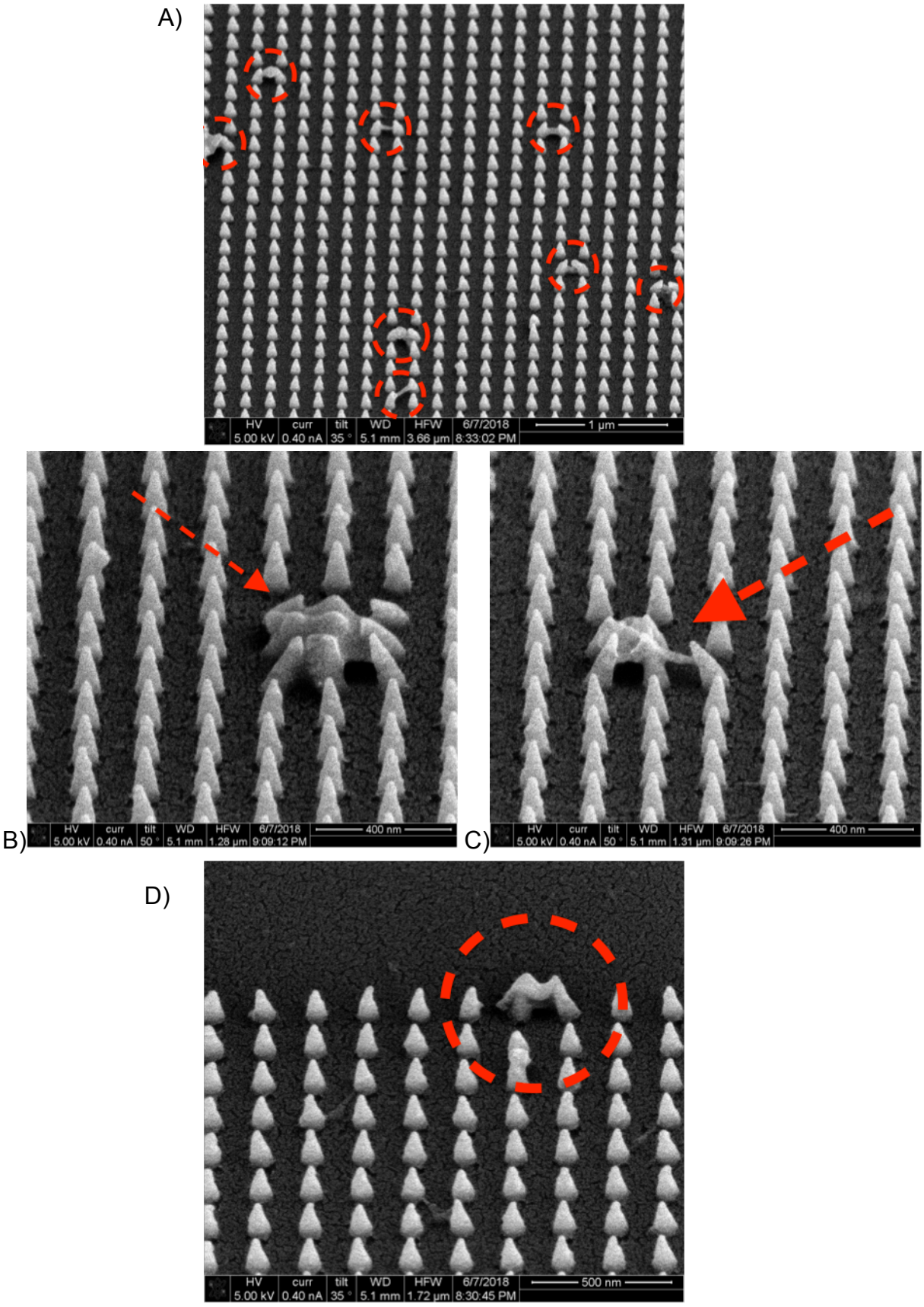


**Figure 22: SEM images of patterned surface incubated with *S. aureus* cells for 18 hours A) Various left over bacterial substances (circles) (scale bar 1 µm) B, C) Left over bacterial substance and bending of the pillars underneath (arrow) (scale bar 400 nm) D) Left over bacterial substance and bending of the pillars underneath (circle) (scale bar 500 nm)**

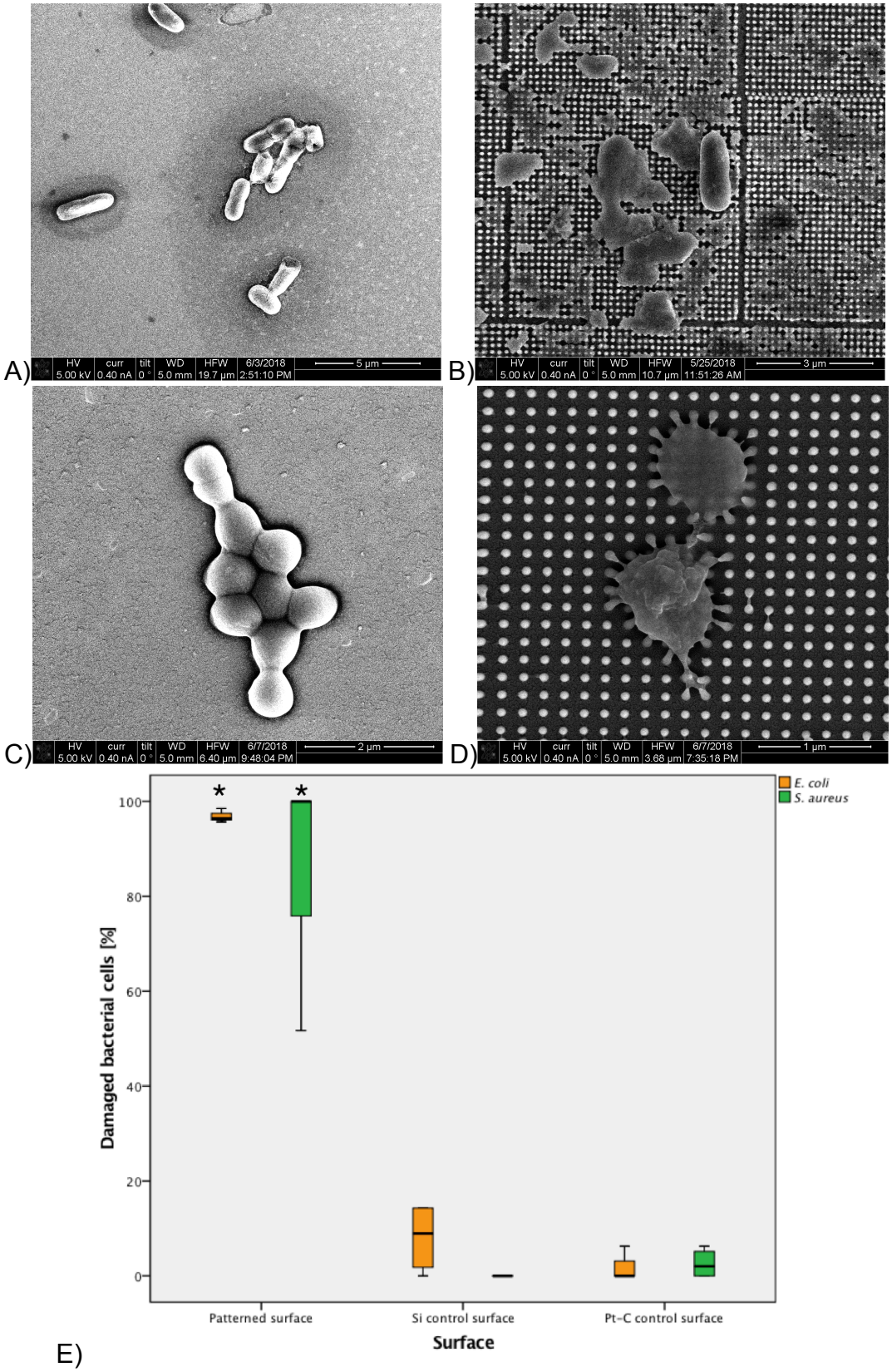


**Figure 23: SEM images exhibiting possible bactericidal efficacy of patterns by (severely) deforming bacterial cells compared to Si control surfaces A) Si control surface incubated with *E. Coli* for 18 hours (scale bar 5 µm) B) Damaged *E. coli* cells on pattern incubated for 18 hours (scale bar 3 µm) C) Si control surface incubated with *S. aureus* for 18 hours (scale bar 2 µm) D) Damaged *S. aureus* cells on pattern incubated for 18 hours (scale bar 1 µm) E) Comparative boxplot graph with percentage damaged bacterial cells on patterned-, Si control- and Pt-C control surfaces. The statistical significance ($p<0.05$) is marked by *, indicating a significant bactericidal difference between patterned surface and Si control surface, and patterned surface and Pt-C control surface.**

# 4 Discussion

## 4.1 Advantages and limitations of pattern fabrication with EBID

Once the surface topography was designed and the pillar dimensions were selected, the process of creating this specified pattern was done with EBID. It took several weeks of trial and error in order to create the patterns with base diameter of ~80 nm, tip diameter of ~20 nm, height of ~190 nm and interpillar distance of ~170 nm by EBID. The results indeed showed that the dimensions could be controlled quite precisely and that this method created reproducible patterns that are within the range of bactericidal features (*appendix A*). According to the statistical analysis there is some variation within the pillar dimensions (*figure 8-11*). Nevertheless, the median values are closely related to the bactericidal features found in literature and to the proposed pattern design *(table 1-2*). However, setting up the right pattern conditions and enlarging the pattern area were challenging.

The pillar dimensions are dependent on both the pattern area and the specific pattern and EBID conditions. When changing only the pattern area (depositing less or more pillars) the dimensions of the pillars change. The reason for this could be that the pillar dimensions are partly dependent on the proximity effects due to increasing collisions of primary-, backscattered- and forward scattered electrons with precursor gas molecules and deposited pillars [21].

In order to create one pattern of 42 by 42 $\mu m^2$ the EBID machine had to be manually controlled for at least 6.5 hours. Including setting up the machine, refocusing and checking the dimensions in between, and patterning the streamfiles one by one, a sample containing 3 patterns took approximately 30 - 36 hours to produce.
When creating larger areas for the purpose of testing the patterns with a higher number of bacteria, human cells and for the end goal of resurfacing the metallic bone implant with nanopillars, it will be a very time-consuming process. Not only will it take more time to pattern the larger areas, the specific pattern conditions have to be adjusted to get similar dimensions.

Even though the process is quite time consuming, EBID showed that patterns could be reproduced. Whereas other methods used by related studies, have shown less controllability of pattern features, especially the interspace distance seemed to be of poor accuracy when using methods like reactive ion etching (RIE) and plasma etching [22-24]. This feature however has a small range (60-200 nm) in which it might help the bactericidal efficacy of the pattern for *E. coli* and *S. aureus* (*table 1*) and thus should be controlled as precise as possible.

In order to create quality patterns with good accuracy in less time, it can be an option to use nano-imprinting. Nano imprint lithography is a low cost, high resolution and high throughput patterning technique that is suitable for the fabrication of single nanometre structures by creating a template stamp of patterns (made by EBID), which can be used to create high quantities of large patterned surfaces [25]. However, the process of creating the stamp still takes quite some time and the substrate has to undergo multiple steps (e.g. adding of resist and primer) in order to be stamped with a pattern.

Another method for sufficiently upscaling patterns could be parallel EBID in which multiple patterns can be deposited simultaneously by using a multi-beam scanning electron microscope [26]. However, this method is still in the experimental phase and has to be improved before it can be successfully incorporated as a new pattern production method.

## 4.2 Bactericidal efficacy of the patterns and potential underlying mechanisms

The SEM images of the incubated patterns showed that most *E. coli* cells are completely deformed and are not recognizable as *E. coli* compared to the control surfaces (*figure 15, 23*). This could be because of multiple severely damaged *E. coli* cells laying closely to each other, since the *E. coli* cells showed an affinity to form clusters (*figure 13-14*). These severe deformations of *E. coli* cells are also in line with different studies that show a significant change in bacterial cell morphology when (nano)pillars exert a large amount of mechanical stress on Gram-negative bacteria, leading to membrane rupture and release of cell contents [18, 27, 28].

The squashed-like, flattened morphology of *S. aureus* on the patterns indicates cell death and was also observed in a study that used nanostructures with tip radius of ~50 nm to puncture *S. epidermidis* [29]. The tip radius of the pillars, used for our experiment, is ± 5 times smaller, which led to higher local stresses on the bacterial wall subsequently increasing the chances of cell wall puncturing.
However, bending of the pillars underneath the damaged bacterial cells was observed in our study (*figure 21-22*) and does not support the cell wall puncturing mechanism (at least not through initial contact). Nevertheless, in order to disclose the puncturing bactericidal mechanism, it might be useful to cut the samples and observe the interaction between the pillar and the (inside of the) bacterial cell.

Most studies showing severely damaged bacterial cells similar to the results of our study report that the bacteria are dead by using live/dead staining in combination with fluorescent microscopy and SEM [11, 29-31]. Thus, the damaged-to-total bacteria ratio might be a good indicator of bactericidal efficacy of the patterns.

The pillars with base diameter of ~80 nm, tip diameter of ~20 nm, height of ~190 nm and interpillar distance of ~170 nm has shown approximately 96.9 ± 1.2% bactericidal efficacy against *E. coli,* whereas this same pattern had approximately 83.9 ± 22.8% bactericidal efficacy against *S. aureus*.
The bactericidal effects of the surface-chemistry were significantly low (*figure 23*), thus it's likely that surface-chemistry dependent cell damage can be ruled out. The bacterial cells on the Si control surfaces showed barely any damages and displayed normal dimensions for *E. coli* and *S. aureus* (*table 6, 9*) [17, 32], this makes it assumable that the used bacterial strains were in healthy conditions and did not affect the bactericidal efficacy of the pattern.

What can be noticed from the statistical analysis (*figure 23)* is the high median value of damaged *S. aureus* cells (100%) compared to the mean value (83.9%). The reason for this large difference can be found in the variance between the three incubated patterns on sample 2. The first pattern on this sample had more clusters of *S. aureus* cells stacked on top of each other. The cells on top showed no damages. This is likely due to the lack of surface-bacteria interaction, which led to a lower bactericidal efficacy of this pattern.
In addition, according to the statistical analysis there was no significant difference between the bactericidal efficacy of the pattern against *E. coli* and *S. aureus* (*figure 23*). Concluding that the pattern is able to kill *E. coli* and *S. aureus* with more of less the same efficacy.

When assuming that the bactericidal effects of the pattern mainly depends on the physical distortion of the cell wall exerted by the pillars, the lower bactericidal efficacy to *S. aureus* is in agreement with the physical properties of these two different bacteria. Gram-positive bacteria, like *S. aureus,* that exhibit a larger stretching modulus compared to Gram-negative bacteria (e.g. *E. coli*) due to their more rigid cell wall, have a higher resistance against the mechanical stresses resulting from the pillars [6, 9, 17].

Due to these differences, it is also possible that the underlying bactericidal mechanisms for these two bacteria types might be different. In the previous paragraph physically puncturing the cell wall had been addressed as a potential bactericidal mechanism.

However, according to recent literature another bactericidal mechanism, based on robust adhesion between secreted EPS of the bacterial cell and the pillars in combination with rising shear forces due to bacterial migration, might explain the EPS found on the patterns incubated with *E. coli* [8, 33].
SEM images of the area close to the patterns also showed damaged *E. coli* cells (*figure 16*). Since the bactericidal effects of the surface-chemistry was significantly low (*figure 23*), meaning the damaging effects of the bacteria surrounding the patterns is most likely not due to platinum-carbon contamination of the EBID process, there is reason to believe that the *E. coli* cells indeed tried to move to a surface that was less stressful. The damage done by the pillars might have been so severe that escaping the patterned surface did not lead to survival of the *E. coli* cells.

The study that proposed this mechanism had found the same severity in bacterial morphology deformation and bacterial cell content (after 4 hours of incubation) and showed that this content found on the patterned surface was a mixture of *E. coli* substances (EPS, cell membranes and cytoplasm) [33].

However, when looking at the area around the patterns incubated with *S. aureus* there are almost no damaged cells observed (*figure 20*). This is most likely due to the non-motile nature of *S. aureus*, which prevents the bacterial cell to move to another spot on the surface [6].

In contrary to that believe, bending of the pillars underneath the *S. aureus* cells and left over bacterial substances on the pillars (*figure 21-22*) initiate the hypothesis that the non-motile *S. aureus* does prefer to migrate from the disparaging pillars.

The reason for the shift from non-motile to motile could be caused by genetic change triggered by stress-induced defence mechanisms [34]. However, it might not be able to move far enough to dodge the pillars.
Bending of the pillars in combination with left over (EPS) substances was also found in a study performed by Bandara et al, 2017 [33].
Thus, the proposed mechanism, that combines the pillar related stress with EPS adhesion and the tendency of bacteria to migrate from the unfavourable pillars, might be the underlying bactericidal mechanism of the pattern with pillar base diameter of ~80 nm, tip diameter of ~20 nm, height of ~190 nm and interpillar distance of ~170 nm. This mechanism can suffice for both *E. coli* and *S. aureus.*

The difference between severities of deformation of the two bacterial cells types can be due to faster cell death of *E. coli* (lower resistance to mechanical stresses due to thinner cell membrane) and higher motility (increased shear forces). In addition, the degree of morphological deformation of *E. coli* on the patterned surface is similar to the last stage of bacterial cell death, in which the height of the bacteria becomes equal to the pillar height and the cytoplasm has leaked out of the cells and has sunken into the spaces between the pillars [33].

## 4.3 Further research

Conversely to our aim, these large amounts of bacterial contents left on the patterned surface can also be used as a growth medium and/or protective layer for other bacteria and can stimulate biofilm formation [29].
It is unknown whether the hosts immune system could get rid of this debris on the patterned bone implant surface in time to prevent the dead bacterial build up. This could be tested by *in vivo* experiments during which the patterned surface should be monitored inside the host or by focusing on the reaction of leucocytes to the patterns.

In addition, it can be interesting to observe how the host cells react on this pattern by performing human- and/or stem cell experiments. Especially for the purpose of bone implants, it would be important that the host cell does not negatively interfere with the pattern or gets damaged as the bacterial cells, and preferably would stimulate bone formation to increase the stability of the implant. Since some research has been done in osteogenic differentiation of stem cells by nanoscale topography, it can be interesting to evaluate whether this bactericidal pattern might have multibiofunctional properties [1, 5, 35, 36].

Moreover, the *E. coli* damage that has been found on the patterned surface looked similar to the damage found in another study after 4 hours of incubation [25]. Therefore, it might be feasible that the pattern killed the bacteria in a substantially shorter time than 18 hours and is interesting to assess with different-time points experiments.

Thus, it is advised to perform long- and short-term experiments in combination with live imaging of the cells to establish possible (short-) and long-term bactericidal efficacy of topography and gain more insights into the bactericidal mechanism(s).

When performing live imaging of the cells on the samples, the antibiofouling properties that are another approach to creating antibacterial topographies, can also be assessed.
Furthermore, stem cell- and *in vivo* experiments would provide knowledge about the interaction of the pattern with a more clinical relevant environment and might reveal extra pattern advantages.

# 5 Conclusions and outlook

Since the rise of peri-implant infections there has been a need for (bone) implants that can decrease the occurrence of implant related infections through surface topography. These infections are mostly due to Gram-positive *Staphylococcus* bacteria. However, also other bacteria as for example the Gram-negative *Escherichia coli* can increase the biofilm formation on the bone implant surface, potentially resulting in stubborn infections that are difficult to treat.
The aim of this study was to create a surface topography that was able to kill *Escherichia coli* and *Staphylococcus aureus* bacteria. This was a relatively novel research since most studies that focus on bactericidal topography have shown to be highly bactericidal to only one type of bacteria, either Gram-positive or Gram-negative bacteria.
It has been found that a specified surface topography was able to damage approximately 96.9 ± 1.2% of *Escherichia coli* and 83.9 ± 22.8% of *Staphylococcus aureus* cells determined by scanning electron microscopy (SEM). This topography was a pattern of nanopillars with base diameter of ~80 nm, tip diameter of ~20 nm, height of ~190 nm and interpillar distance of ~170 nm produced with electron beam induced deposition (EBID). The severity of bacterial cell damage has led to believe that the percentage of dead bacterial cells was a sufficient measure for the bactericidal efficacy of the pattern. There hasn't been another pattern reported that is able to kill both bacteria with such high efficacy.

The underlying bactericidal mechanism, that might explain these results, is the hypothesis that the pillars trigger strong extracellular polymeric substances (EPS) adhesion of bacterial cells and stimulates the need of the bacteria to migrate from the unfavourable pattern.
This combination of high local stresses and shear forces can lead to severe morphological deformations of the bacterial cell, which eventually results in a final stage of cell death where the height of the bacteria becomes equal to the pillar height and the cytoplasm leaks out of the cells and sinks into the spaces between the pillars.

Based on these results there is convincing prospect that these specified pillar parameters can be used as an effective bactericidal surface topography against the implant-infection associated *Escherichia coli* and *Staphylococcus aureus.*

Nevertheless, more investigation should be done in short and long-term effects of the patterns on bacteria and host cells in combination with live/dead staining and live-imaging. In order to perform these follow-up experiments it is advised to look into other, less time-consuming pattern production methods.

# 6 References


1. Neoh, K.G., et al., *Balancing osteoblast functions and bacterial adhesion on functionalized titanium surfaces.* Biomaterials, 2012. **33**(10): p. 2813-22.
2. Song, Z., et al., *Prosthesis Infections after Orthopedic Joint Replacement: The Possible Role of Bacterial Biofilms.* Orthopedic Reviews, 2013. **5**(2): p. e14.
3. Campoccia, D., L. Montanaro, and C.R. Arciola, *The significance of infection related to orthopedic devices and issues of antibiotic resistance.* Biomaterials, 2006. **27**(11): p. 2331-9.
4. Bhadra, C.M., et al., *Antibacterial titanium nano-patterned arrays inspired by dragonfly wings.* Scientific Reports, 2015. **5**: p. 16817.
5. Zhu, C., et al., *Antimicrobial design of titanium surface that kill sessile bacteria but support stem cells adhesion.* Applied Surface Science, 2016. **389**(Supplement C): p. 7-16.
6. Elbourne, A., R.J. Crawford, and E.P. Ivanova, *Nano-structured antimicrobial surfaces: From nature to synthetic analogues.* J Colloid Interface Sci, 2017. **508**: p. 603-616.
7. Anselme, K., et al., *The interaction of cells and bacteria with surfaces structured at the nanometre scale.* Acta Biomater, 2010. **6**(10): p. 3824-46.
8. Viela, F., et al., *Moth eye mimetic cytocompatible bactericidal nanotopography: A convergent design.* Bioinspir Biomim, 2018.
9. Sengstock, C., et al., *Structure-related antibacterial activity of a titanium nanostructured surface fabricated by glancing angle sputter deposition.* Nanotechnology, 2014. **25**(19): p. 195101.
10. Widyaratih, D.S., *Bacterial Cells Response to Osteogenic Nanopatterns.* Delft University of Technology repository, 2017.
11. Wu, S., et al., *Nanostructured surface topographies have an effect on bactericidal activity.* J Nanobiotechnology, 2018. **16**(1): p. 20.
12. Dickson, M.N., et al., *Nanopatterned polymer surfaces with bactericidal properties.* Biointerphases, 2015. **10**(2): p. 021010.
13. Ivanova, E.P., et al., *Natural bactericidal surfaces: mechanical rupture of Pseudomonas aeruginosa cells by cicada wings.* Small, 2012. **8**(16): p. 2489-94.
14. Linklater, D.P., et al., *Influence of nanoscale topology on bactericidal efficiency of black silicon surfaces.* Nanotechnology, 2017. **28**(24): p. 245301.
15. Bhadra, C.M., et al., *Subtle Variations in Surface Properties of Black Silicon Surfaces Influence the Degree of Bactericidal Efficiency.* Nano-Micro Letters, 2018. **10**(2).
16. van Dorp, W.F., et al., *Approaching the Resolution Limit of Nanometer-Scale Electron Beam-Induced Deposition.* Nano Letters, 2005. **5**(7): p. 1303-1307.
17. Tripathy, A., et al., *Natural and bioinspired nanostructured bactericidal surfaces.* Advances in Colloid and Interface Science, 2017. **248**: p. 85-104.
18. Linklater, D.P., S. Juodkazis, and E.P. Ivanova, *Nanofabrication of mechano-bactericidal surfaces.* Nanoscale, 2017. **9**(43): p. 16564-16585.
19. Silvis-Cividjian, N. and C.W. Hagen, *Electron‐Beam‐Induced Nanometer‐Scale Deposition*, in *Advances in Imaging and Electron Physics*. 2006, Elsevier. p. 1-235.
20. Dobbenga, S., et al., *NANOPATTERN-MEDIATED POKING OF THE PLASMA MEMBRANE: NATURE'S TOUCH SCREEN?* 2017.

21. Utke, I., P. Hoffmann, and J. Melngailis, *Gas-assisted focused electron beam and ion beam processing and fabrication.* Journal of Vacuum Science & Technology B, Nanotechnology and Microelectronics: Materials, Processing, Measurement, and Phenomena, 2008. **26**(4).
22. May, P.W., et al., *Diamond-coated 'black silicon' as a promising material for high-surface-area electrochemical electrodes and antibacterial surfaces.* Journal of Materials Chemistry B, 2016. **4**(34): p. 5737-5746.
23. Hizal, F., et al., *Impact of 3D Hierarchical Nanostructures on the Antibacterial Efficacy of a Bacteria-Triggered Self-Defensive Antibiotic Coating.* ACS Appl Mater Interfaces, 2015. **7**(36): p. 20304-13.
24. Wu, S., et al., *Antibacterial Au nanostructured surfaces.* Nanoscale, 2016. **8**(5): p. 2620-5.
25. Scotuzzi, M., T. Glinser, and C.W. Hagen, *EBID stamps for Nano Imprint Lithography.* 2017.
26. Post, P.C., et al., *Parallel electron-beam-induced deposition using a multi-beam scanning electron microscope.* Journal of Vacuum Science & Technology B, 2011. **29**(6).
27. Pogodin, S., et al., *Biophysical model of bacterial cell interactions with nanopatterned cicada wing surfaces.* Biophys J, 2013. **104**(4): p. 835-40.
28. Li, X., *Bactericidal mechanism of nanopatterned surfaces.* Phys Chem Chem Phys, 2016. **18**(2): p. 1311-6.
29. Cao, Y., et al., *Nanostructured titanium surfaces exhibit recalcitrance towards Staphylococcus epidermidis biofilm formation.* Scientific Reports, 2018. **8**(1).
30. Ivanova, E.P., et al., *Bactericidal activity of black silicon.* Nat Commun, 2013. **4**: p. 2838.
31. Hasan, J., et al., *Multi-scale surface topography to minimize adherence and viability of nosocomial drug-resistant bacteria.* Mater Des, 2018. **140**: p. 332-344.
32. Foster, T., *Staphylococcus*, in *Medical Microbiology*, S. Baron, Editor. 1996: Galveston (TX): University of Texas Medical Branch at Galveston.
33. Bandara, C.D., et al., *Bactericidal Effects of Natural Nanotopography of Dragonfly Wing on Escherichia coli.* ACS Applied Materials & Interfaces, 2017. **9**(8): p. 6746-6760.
34. Rizzello, L., et al., *Impact of nanoscale topography on genomics and proteomics of adherent bacteria.* ACS Nano, 2011. **5**(3): p. 1865-76.
35. Dobbenga, S., L.E. Fratila-Apachitei, and A.A. Zadpoor, *Nanopattern-induced osteogenic differentiation of stem cells - A systematic review.* Acta Biomater, 2016. **46**: p. 3-14.
36. Klymov, A., et al., *Understanding the role of nano-topography on the surface of a bone-implant.* Biomaterials Science, 2013. **1**(2): p. 135-151.

# Appendices

## Appendix A

Additional SEM images and measurements of patterns, containing nanopillars, made at different locations on the patterned samples.

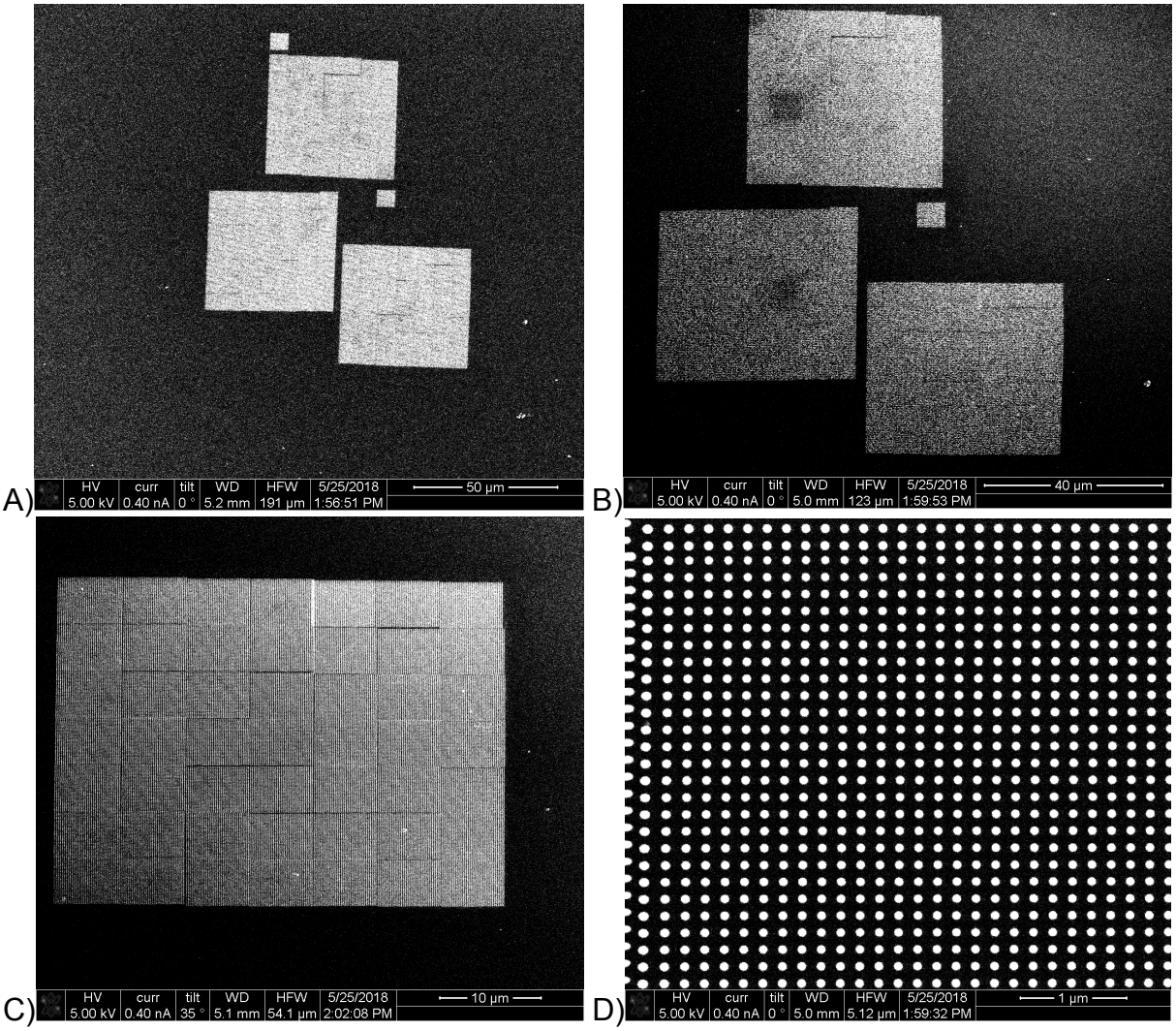


**Figure 24: SEM images A) Overview image of three patterned surfaces, each pattern occupying an area of 42 x 42 µm$^2$ and two smaller test patterns of 6 x 6 µm$^2$ (scale bar 50 µm) B) Overview image of three patterned surfaces, each pattern occupying an area of 42 x 42 µm$^2$ and two smaller test patterns of 6 x 6 µm$^2$ (scale bar 40 µm) C) Overview image of one pattern of 42 x 42 µm$^2$ (scale bar 10 µm) D) Top view image of pattern (scale bar 1 µm)**

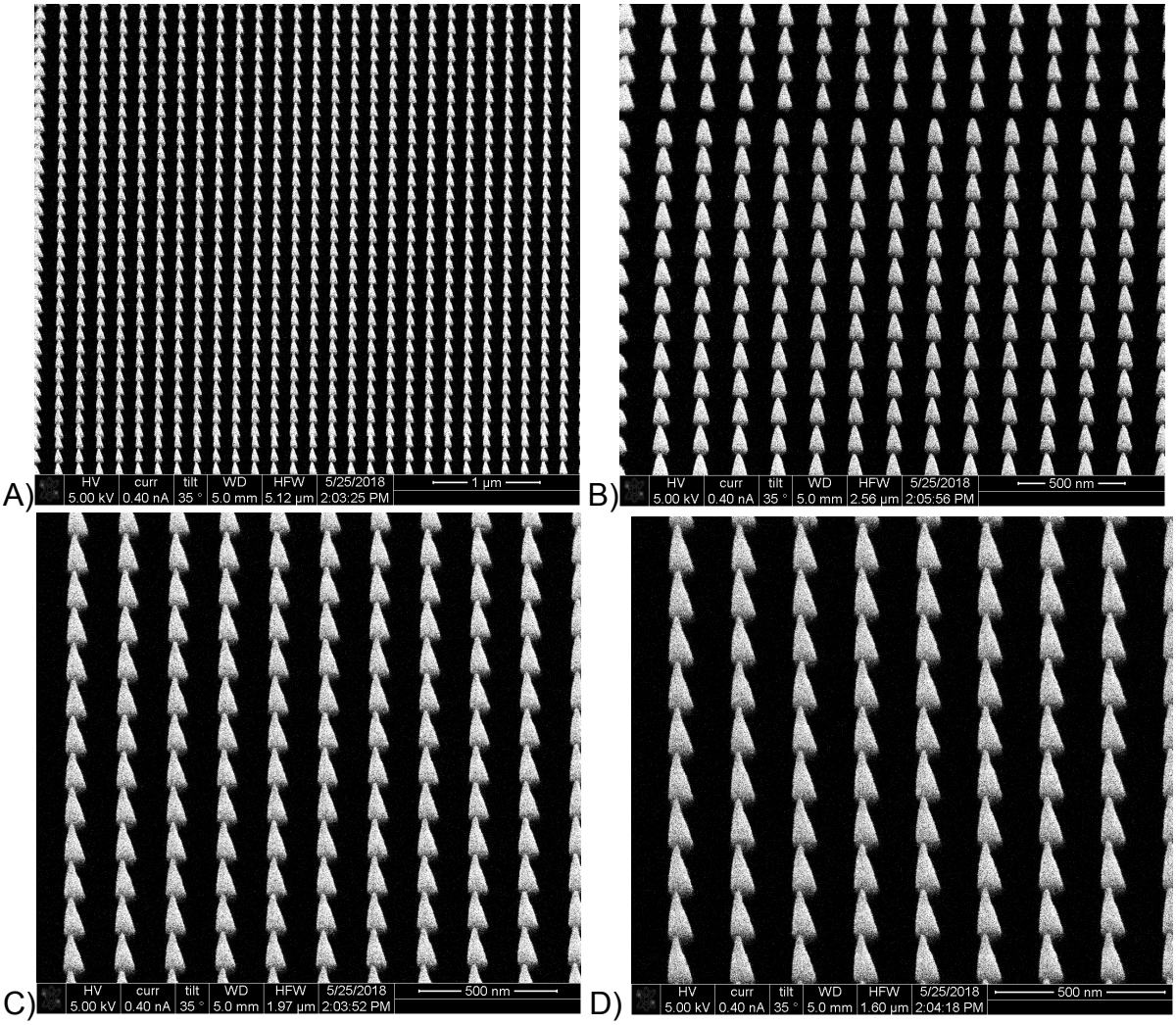


**Figure 25: SEM images A) Tilted image of pattern (scale bar 1 µm) B) Tilted image of pattern (scale bar 500 nm) C) Tilted image of pattern (scale bar 500 nm) D) Tilted image of pattern (scale bar 500 nm)**

Table 12: mean base diameter, tip diameter, height and interpillar distance of the produced patterns on sample 1 including standard deviation

| Nanopatterns sample 1 | Mean base diameter [nm] | Mean tip diameter [nm] | Mean height [nm] | Mean interpillar distance [nm] |
|---|---|---|---|---|
| 1 | 75.09 ± 3.65 | 22.61 ± 3.61 | 186.95 ± 6.88 | 170.75 ± 2.06 |
| 2 | 74.26 ± 3.42 | 21.30 ± 2.15 | 182.98 ± 8.13 | 170.75 ± 1.26 |
| 3 | 85.09 ± 4.89 | 22.49 ± 2.60 | 188.02 ± 5.95 | 169.75 ± 1.50 |
| **Combined** | **78.14 ± 6.37** | **22.13 ± 2.90** | **185.98 ± 7.33** | **170.42 ± 1.56** |

Table 13: mean base diameter, tip diameter, height and interpillar distance of the produced patterns on sample 2 including standard deviation

| Nanopatterns sample 2 | Mean base diameter (nm) | Mean tip diameter (nm) | Mean height (nm) | Mean interpillar distance [nm] |
|---|---|---|---|---|
| 1 | 72.63 ± 3.15 | 20.48 ± 3.18 | 179.85± 6.60 | 170.79 ± 3.16 |
| 2 | 71.68 ± 2.50 | 19.70 ± 2.72 | 185.58 ± 7.76 | 173.08 ± 2.95 |
| 3 | 71.47 ± 2.89 | 18.79 ± 2.12 | 186.61 ± 6.47 | 177 ± 2.77 |
| **Combined** | **71.92 ± 2.88** | **19.65 ± 2.78** | **184.04 ± 7.54** | **173.57 ± 3.97** |

Table 14: mean base diameter, tip diameter, height and interpillar distance of the produced patterns on sample 3 including standard deviation

| Nanopatterns sample 3 | Mean base diameter (nm) | Mean tip diameter (nm) | Mean height (nm) | Mean interpillar distance [nm] |
|---|---|---|---|---|
| 1 | 74.02 ± 2.57 | 20.91 ± 2.78 | 187.69 ± 5.92 | 169.75 ± 1.50 |
| 2 | 76.07 ± 3.13 | 21.89 ± 2.34 | 184.77 ± 9.16 | 170.25 ± 1.50 |
| 3 | 75.02 ± 2.99 | 20.23 ± 1.80 | 188.82 ± 9.11 | 169.5 ± 1.73 |
| **Combined** | **75.04 ± 3.01** | **21.01 ± 2.43** | **187.10 ± 8.34** | **169.83 ± 1.47** |

# Appendix B

Bacterial growth curves of *E. coli* and *S. aureus* performed in duplicates. A 24-well plate was incubated for 15 hours at 37 °C with both bacteria in Lysogeny-broth (LB) and Brain Heart Infusion broth (BHI). OD measurements were automatically taken for every 10 minutes.

The results showed that in BHI medium both bacteria obtain faster growth rates and higher growth after 15 hours, which indicates that BHI is a more nutritious medium than LB. However, LB is the widely used medium for *E. coli* and BHI for *S. aureus*. Thus, for the experiments during this study we relied on the protocols of the manufacturer (*BEI Resources*).

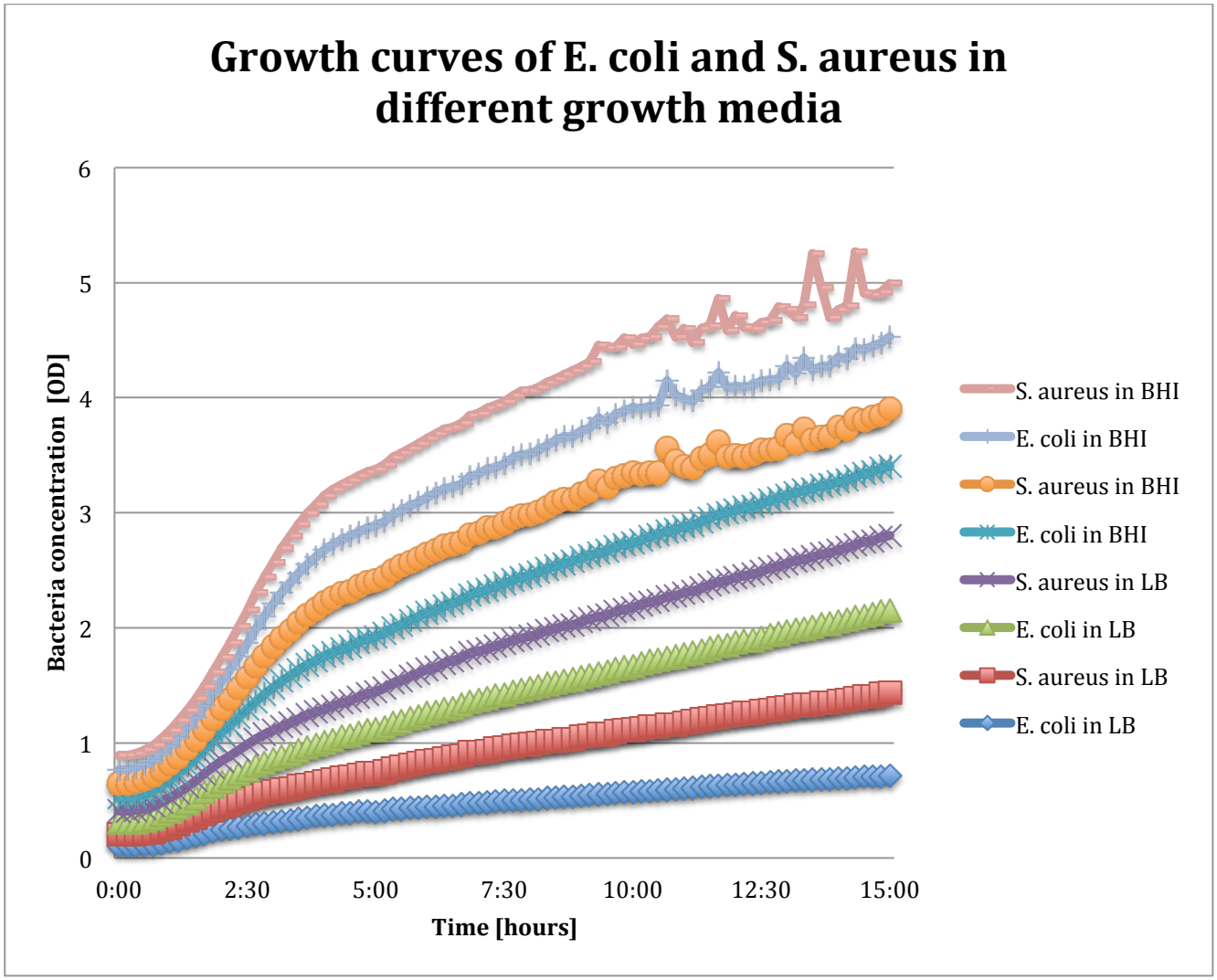


**Figure 26: Growth curves of *E. coli* and *S. aureus* incubated for 15 hours in a 24-well plate with BHI and LB media**